DEVELOPMENT OF AN IN-SITU METHOD FOR CONTINUOUS EVALUATION OF THE RESILIENT MODULUS OF PAVEMENT SUBGRADE

by

MICHAEL P. RITS, B.S

REPORT

Presented to the Faculty of the Graduate School of

The University of Texas at Austin

in Partial Fulfillment

of the Requirements

for the Degree of

MASTER OF SCIENCE IN ENGINEERING

THE UNIVERSITY OF TEXAS AT AUSTIN

December 1992

1992 THESIS/DISSERTATION

Development of an In-Site Method for Continuous Evaluation of the Resilient Modulus of Pavement Subgrade

Captain Michael P. Rits

AFIT Student Attending: University of Texas

AFIT/CI/CIA-92-120

AFIT/CI
Wright-Patterson AFB OH 45433-6583

ABSTRACT

FOR

DEVELOPMENT OF AN IN-SITU METHOD FOR CONTINUOUS EVALUATION OF THE RESILIENT MODULUS OF PAVEMENT SUBGRADE

by

MICHAEL P. RITS, B.S
CAPT, USAF

MAJOR REPORT
(100 Pages)

Presented to the Faculty of the Graduate School of

The University of Texas at Austin

In Partial Fulfillment

of the Requirements

for the Degree of

MASTER OF SCIENCE IN ENGINEERING

from

THE UNIVERSITY OF TEXAS AT AUSTIN

1992

1. Objective: Pavement designs, materials and uses vary around the world, but engineers typically employ the resilient moduli of pavement materials as the primary means of evaluating those materials. Unfortunately, the majority of tests used to determine the resilient modulus of materials are performed in the laboratory where the material either has been removed from the in-situ conditions or has been reconstituted. Soil samples which are removed from the ground using various techniques are at best moderately disturbed. Typically the testing of these samples is performed in a triaxial device equipped for repetitive axial loading. The strain used to calculate the resilient modulus is the recoverable portion of the deformation response. The fact that this response varies with state of stress is widely accepted, but the laboratory test results continue to be used for lack of a more useful and convenient method of determining resilient moduli (Yoder and Witczak, 1975).

The purpose of this study is to develop a method for continuous, in-situ evaluation of the resilient modulus of subgrade material under a highway pavement using seismic waves. Although this technique is not mobile and the equipment is fully embedded in the soil under the pavement, it provides a more accurate means of evaluating resilient modulus. This approach can then be used as a benchmark with which to compare the laboratory results to improve design methods as well as our fundamental understanding of the behavior of pavement materials in the field.

2. Scope: The scope of this study involves development of the field approach and analysis of the field data. The work included development of an array of 12 geophones. Geophones are electromechanical transducers which can transmit or receive vibrations within their calibrated frequency range and therefore can be used as both sources and receivers for the stress (seismic) waves. The work included: 1. the fabrication, calibration and placement of the geophones in the soil subgrade in the proper orientation, 2. measurements of the shear and constrained compression wave velocities under imposed stress conditions, and 3. interpretation of the raw data to determine resilient moduli.

Also involved in the primary research are the measurement of negative pore water pressures in the soil subgrade, evaluation of the modulus of elasticity of the asphalt surface layer using the Spectral-Analysis-of-Surface-Waves method, measurement of several statically imposed wheel loads, and

determination of the soil subgrade characteristics in terms of total unit weight, water content and Atterberg limits. The study was performed in coordination with a Texas DOT project, and the results will have direct application to the evaluation of newly constructed pavement systems.

3. Summary of Results: Using stress wave velocities found from seismic testing, the shear and constrained moduli and Poisson's ratio were determined in the three orthogonal directions. The average wave velocities with no added surface load measured in this study are shown in Table 1.

Wave Type	Geophone	Wave Velocity (fps)
P	8-9	1203
SH	7-8	641
SH	11-12	577
SV	13-14	584
SH	2-5	559
P	1-17	1301

Table 1: Average Wave Velocities from Seismic Measurements with No Added Surface Load

The resilient modulus of the subgrade in the vertical direction was found to be approximately 22,500 psi (155 MPa) by measuring the body wave velocities in the subgrade, as shown in Figure 2.

Orientation	Geophone Pairs		Poisson's Ratio	Modulus of Elasticity (psi)
	P-Wave	S-Wave		
East-West	8/9	11/12	0.35	23,436
North-South	-	7/8	0.35	28,970
Vertical	1/17	2/5	0.38	22,494

Table 2: Comparison of E and ν in Three Directions Using Average Wave Velocities from Seismic Measurements with No Added Surface Load

The soil appeared to be stiffer in the direction perpendicular to traffic (probably due to the direction of compaction) and also stiffer in the vertical plane than in the horizontal plane.

Little difference was measured in the wave velocities with increasing vertical effective stress, except with the geophone pair 1/17. For this pair, the P-wave velocities increased from approximately 1300 fps (396 m/s) to 1400 fps (427 m/s) with relatively small increases in effective stress.

With already proven field techniques and relatively inexpensive equipment, many seismic tests can be run in a short period of time, or over the long term, to determine the resilient modulus. As the need for more cost effective pavement designs increases, the degree of accuracy of knowing the properties of the materials increases. Dynamic, in-situ testing will improve the knowledge of some of the most important soil properties used in designing pavement systems.

REFERENCES

Aouad, M. F., K. H. Stokoe, II, and R. C. Briggs (1992) *Stiffness of the Asphalt Concrete Surface Layer from Stress Wave Measurements*, Paper Prepared for Presentation to the 1993 Annual Meeting of the Transportation Research Board, University of Texas at Austin

Hardin, B. O. and V. P. Drnevich (1972) *Shear Modulus and Damping in Soils: Design Equations and Curves*, Journal of the Soil Mechanics and Foundations Division, ASCE, Vol. 98, No. SM7, pp. 667-692.

Richart, F. E., Jr., J. R. Hall, Jr., and R. D. Woods (1970) *Vibrations of Soils and Foundations*, Prentice-Hall, Inc., Englewood Cliffs, N. J.

Seed, H. B. and I. M. Idriss (1970) *Soil Moduli and Damping Factors for Dynamic Response Analysis*, Earthquake Engineering Research Center Report, EERC 70-10.

Stannard, David I (1986) *Theory, Construction and Operation of Simple Tensiometers*, Ground Water Monitoring Review, Vol. 6, No. 3, pp. 70-78.

Stokoe, K. H. II, J. N. Lee, and S. H. Lee (1991) *Characterization of Soil in Calibration Chambers with Seismic Waves*, Calibration Chamber Testing, Edited by An-Bin Huang, Proceedings of the First International Symposium on Calibration Chamber Testing/ISOCCTI, Potsdam, N. Y., pp. 363-376.

Stokoe, K. H., II (1980) *Field Measurement of Dynamic Soil Properties*, Presented to the Specialty Conference on Civil Engineering and Nuclear Power, ASCE, Sept. 15-17, Knoxville, TN, 31 p.

Stokoe, K. H., II and R. J. Hoar (1978) *Variables Affecting In Situ Seismic Measurements*, Proceedings of the Conference on In-Situ Measurement of Soil Properties, ASCE, Vol. II, pp. 919-939.

Yoder, E. J. and M. W. Witczak (1975) *Principles of Pavement Design*, 2nd Ed., John Wiley and Sons, Inc., pp. 40-41.

Dedicated to my loving wife, Kelley

ACKNOWLEDGMENTS

I would like to express my sincere appreciation to my advisor, Professor Kenneth H Stokoe, II, for his patience, helpfulness and expertise in the field of soil dynamics (and general mucking about) In addition, this study would not have been possible without the selfless assistance of doctoral candidates Marwan Aouad, James Bay and Ron Andrus They are experts in their own right and willingly shared with me their knowledge and depth of experience of seismic testing I would like to thank my additional reader, Professor B Frank McCullough, for his time and expertise, and hope that this study will be of much help to the Center for Transportation Research in the future

Several personnel in the Texas Department of Transportation were very helpful and their efforts are much appreciated. In particular, Robert Briggs of the Pavements Design Section and Maureen Wakeland, a construction inspector for the Highway 183 project, provided outstanding coordination and support during the field installation and testing Sergeant Cummings, from the Department of Public Safety, License and Weight Division, was extremely helpful in providing the wheel-load scale for the duration of the testing period

And finally, I thank my wife, Kelley, who endured my long nights of typing, cheered me up when I got discouraged, and lovingly urged me to spend precious time with my children. I would also like to thank all the taxpayers who graciously paid for my education through the United States Air Force

18 September 1992

TABLE OF CONTENTS

ACKNOWLEDGMENTS.....vi

TABLE OF CONTENTS.....vii

CHAPTER 1: INTRODUCTION.....1

CHAPTER 2: BACKGROUND.....3

2.1 WAVE PROPAGATION THEORY.....3

2.2 SEISMIC TESTING TECHNIQUES WITH BODY WAVES.....5

2.3 EFFECT OF STATE OF STRESS IN CALIBRATION CHAMBER TESTS.....7

2.4 USE OF WAVE VELOCITIES TO EVALUATE SOIL STIFFNESS.....12

2.5 EFFECTS OF OVERCONSOLIDATION AND PLASTICITY INDEX.....13

CHAPTER 3: EXPERIMENTAL DESIGN AND FIELD TESTING.....15

3.1 EQUIPMENT.....15

3.2 PAVEMENT MATERIAL PROPERTIES.....29

3.3 SITE DESCRIPTION.....38

3.4 SEISMIC TESTING PROCEDURES.....42

CHAPTER 4: ANALYSIS OF DATA.....47

4.1 DETERMINATION OF WAVE VELOCITIES.....47

4.2 CALCULATION OF SHEAR AND CONSTRAINED MODULI OF THE SOIL SUBGRADE.....49
4.3 CALCULATION OF POISSON'S RATIOS AND RESILIENT MODULI OF THE SOIL SUBGRADE WITH NO ADDITIONAL SURFACE LOAD.....55
4.4 ANISOTROPY OF THE COMPACTED SOIL SUBGRADE WITH NO ADDED SURFACE LOADS.....56
4.5 CALCULATION OF STATE OF STRESS UNDER ADDED LOADS USING LAYERED PAVEMENT THEORY.....58
4.6 COMPARISON OF SHEAR MODULUS WITH THE EMPIRICAL MAXIMUM SHEAR MODULUS.....73

CHAPTER 5: CONCLUSIONS/APPLICATIONS.....76
APPENDIX A: SAMPLE TIME RECORDS MEASURED DURING SEISMIC TESTING.....80
APPENDIX B: CALIBRATION CURVES FOR TIME DELAYS ASSOCIATED WITH EACH GEOPHONE PAIR.....89
REFERENCES.....96

CHAPTER 1

INTRODUCTION

1.1. Background: Pavement designs, materials and uses vary around the world, but engineers typically employ the resilient moduli of pavement materials as the primary means of evaluating those materials. Unfortunately, the majority of tests used to determine the resilient modulus of materials are performed in the laboratory where the material either has been removed from the in-situ conditions or has been reconstituted. Soil samples which are removed from the ground using various techniques are at best moderately disturbed. Typically the testing of these samples is performed in a triaxial device equipped for repetitive axial loading. The strain used to calculate the resilient modulus is the recoverable portion of the deformation response. The fact that this response varies with state of stress is widely accepted, but the laboratory test results continue to be used for lack of a more useful and convenient method of determining resilient moduli (Yoder and Witczak, 1975).

1.2 Objective: The main purpose of this study is to develop a method for continuous, in-situ evaluation of the resilient modulus of subgrade material under a highway pavement using seismic waves. Although this technique is not mobile and the equipment is fully embedded in the soil under the pavement, it provides a more accurate means of evaluating resilient modulus. This approach can then be used as a benchmark with which to compare the laboratory results to improve design methods as well as our fundamental understanding of the behavior of pavement materials in the field.

1.3 Scope: The scope of this study involves development of the field approach and analysis of the field data. The work included development of an array of 12 geophones. Geophones are electromechanical transducers which can transmit or receive vibrations within their calibrated frequency range and therefore can be used as both sources and receivers for the stress (seismic) waves. The work included: 1. the fabrication, calibration and placement of the geophones in the soil subgrade in the proper orientation, 2. measurements of the shear and constrained compression wave velocities (see description in Sections 2.1.1 and 2.1.2) under imposed stress conditions, and 3. interpretation of the raw data to determine resilient moduli.

Also involved in the primary research are the measurement of negative pore water pressures in the soil subgrade, evaluation of the modulus of elasticity of the asphalt surface layer using the Spectral-Analysis-of-Surface-Waves method (see description in Section 3.2.4), measurement of several statically imposed wheel loads, and determination of the soil subgrade characteristics in terms of total unit weight, water content and Atterberg limits. The study was performed in coordination with a Texas DOT project, and the results will have direct application to the evaluation of newly constructed pavement systems.

CHAPTER 2
BACKGROUND

The theory involving stress (seismic) wave propagation has been extensively tested and proven in the field. This particular project is rather unique in that it applies the theory to determine with permanently embedded sources and receivers the in-situ soil stiffness and states of stress at various times after construction. The theories used in this study are described in the subsequent sections.

2.1 Wave Propagation Theory: Two types of waves can be generated in a body: constrained compression waves (P-waves) and shear waves (S-waves). These waves are termed body waves because they propagate through the interior or body of a mass (such as soil subgrade). This is in contrast to surface waves, which only propagate along the surface of a body or mass of soil (Richart et al, 1970).

2.1.1 Constrained Compression Waves in an Elastic Half Space: Compression waves generate particle motion in the soil parallel to the direction in which the waves are propagating as illustrated in Figure 2.1. The compression waves, hereafter referred to as P-waves, are constrained in the directions perpendicular to the direction of wave propagation (Richart et al, 1970).

2.1.2 Shear Waves in an Elastic Half Space: Shear waves generate particle motion perpendicular to the direction of wave propagation, which creates a distortion in the soil laterally as illustrated in Figure 2.2. If the particle motion is contained

in the vertical plane, the wave is referred to as a vertically polarized shear wave, or SV-wave. Likewise, if the particle motion is contained in the horizontal plane, the wave is referred to as a horizontally polarized shear wave, or SH-wave (Richart et al, 1970).

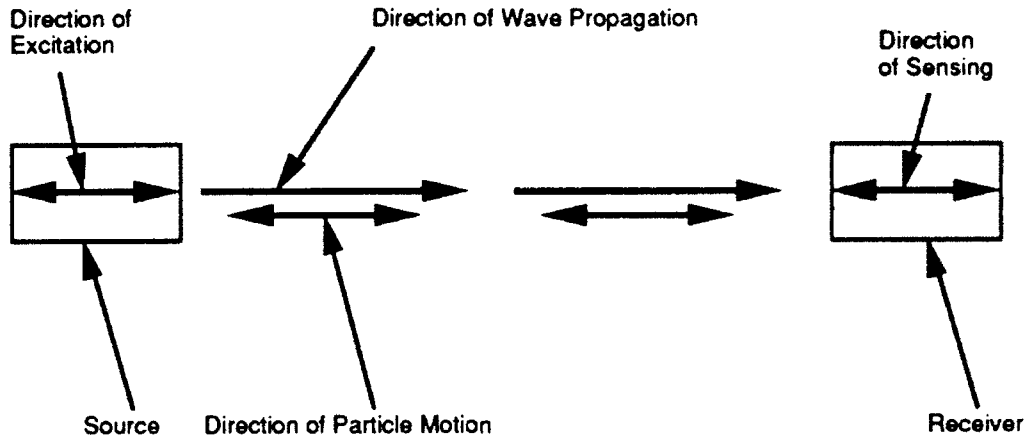

Figure 2.1: Generation and Detection of P-Waves

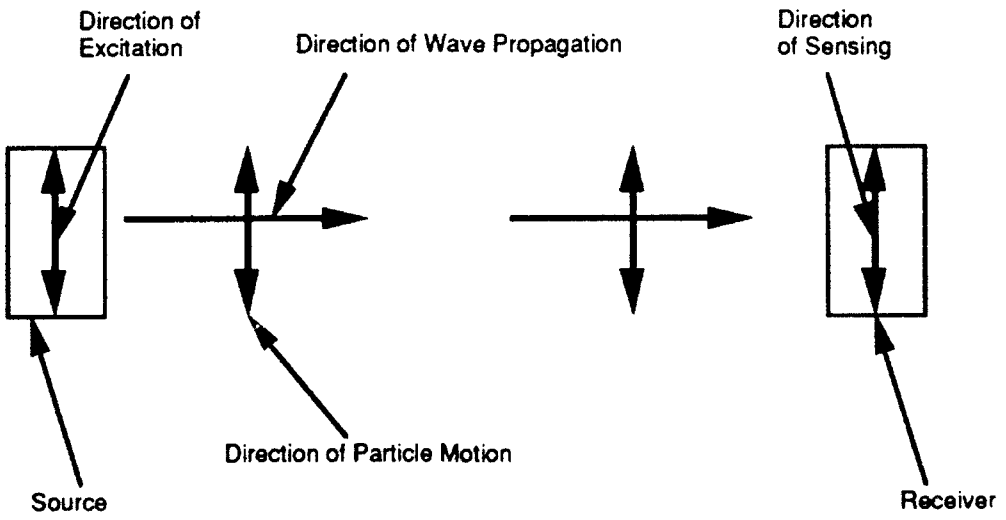

Figure 2.2: Generation and Detection of S-Waves

2.2 Seismic Testing Techniques with Body Waves: The two most widely used techniques for determining P- and S-wave velocities in-situ are the crosshole and downhole methods. Each test requires energy sources which are strong and repeatable for both S-wave and P-wave generation, properly oriented receivers with good coupling with the soil and proper frequency response, appropriate recording equipment, proper data collection and analysis procedures, and well-trained, conscientious field personnel (Stokoe, 1980)

2.2.1 Crosshole Tests: In the crosshole technique, the time for P-waves and S-waves to travel between points of known distances at the same depth are measured (Stokoe and Hoar, 1978). The crosshole test requires at least two or three boreholes as shown in Figure 2.3. A typical time record from a geophone and a source wedged in two cased boreholes is shown in Figure 2.4.

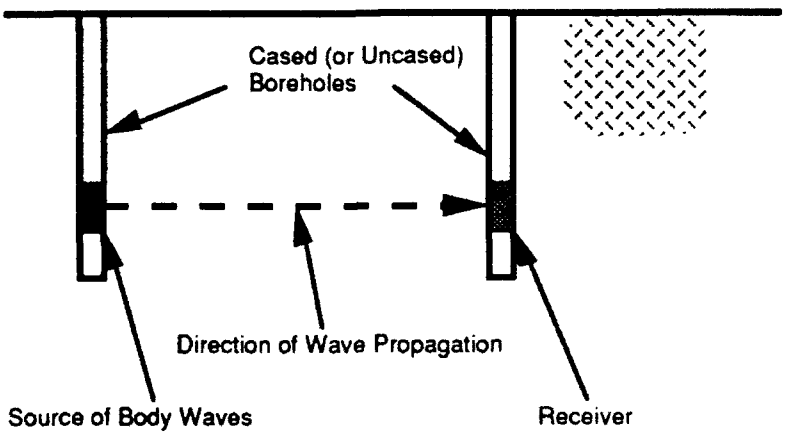

Figure 2.3: Schematic of a Crosshole Seismic Test

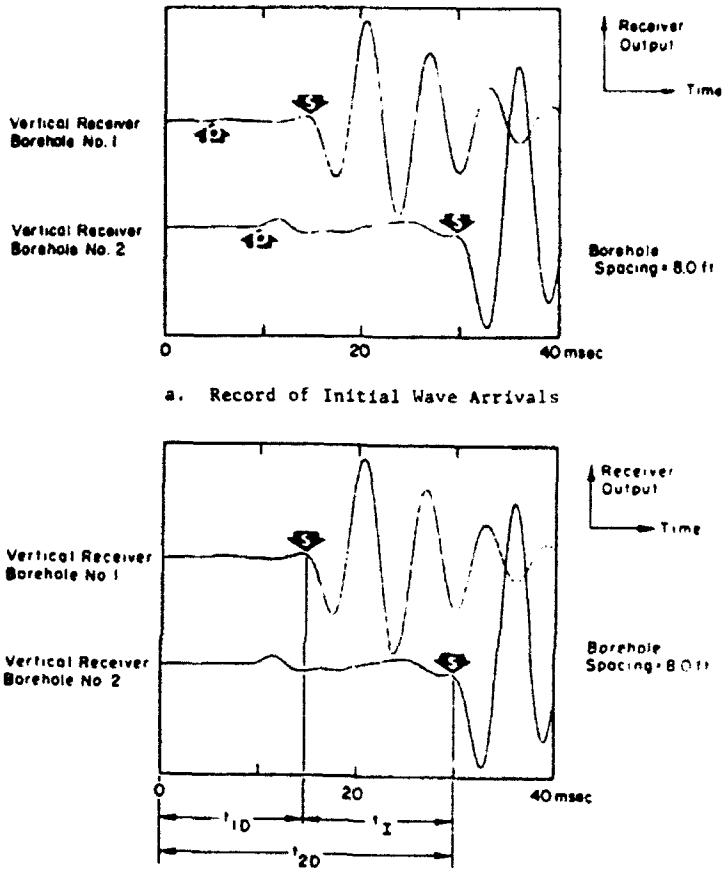

Figure 2.4: Typical Time Record for Seismic Crosshole Test for Two Geophones (Stokoe and Hoar, 1978)

The travel time of the wave is the difference in time between the first arrivals of each wave form. Using the travel times and the distances traveled, the respective wave velocities are calculated.

2.2.2 Down/Up-Hole Tests: In the downhole or uphole technique, the procedure is similar to the crosshole technique, except that the source and receiver are not at the same depth and only one borehole is required as shown in Figure 2.5. Typical time records are similar to the records shown in Figure 2.4. This method provides a means of looking at the soil variability with depth (Stokoe and Hoar, 1978).

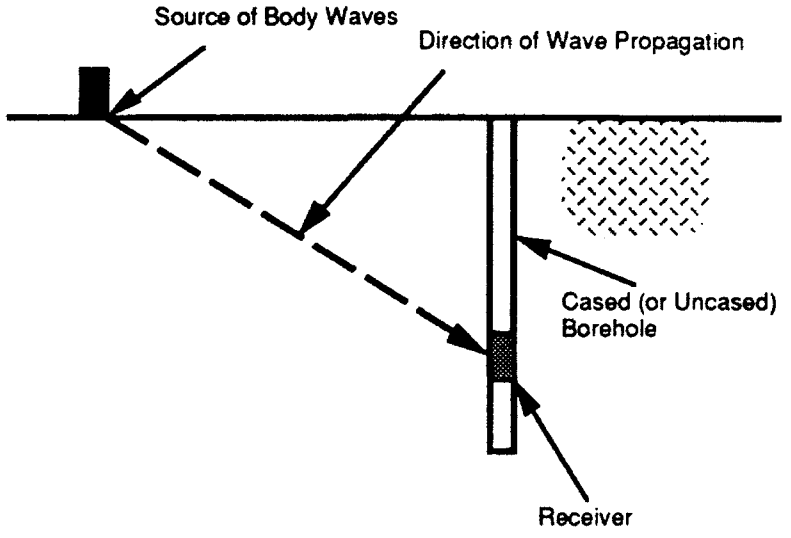

Figure 2.5: Schematic of a Downhole Seismic Test

2.3 Effect of State of Stress on P- and S-Wave Velocities: Calibration chambers have been used to load carefully constructed samples of soil with known boundary conditions. A large cubical calibration chamber was built at the University of Texas in 1979 to conduct basic studies in seismic wave propagation under three-dimensional states of stress. In this chamber, 7 x 7 x 7-ft (2 x 2 x 2-m) cubes of sand were

loaded under various states of stress, with principle effective stresses ranging from 4 to 45 psi (28 to 310 KPa).

The results of the calibration chamber tests showed that both P- and S-wave velocities increased with increasing isotropic confining pressure as shown in Figure 2.6. Each wave velocity shown in Figure 2.6 is designated by a two-letter subscript; the first indicating the direction of wave propagation, and the second indicating the direction of particle motion. The effect of increasing isotropic confining pressure on the wave velocities can show the structural anisotropy of the soil, since the wave velocities will increase similarly if there is isotropy. This relationship is expressed for P-waves as:

$$V_p = C_1 \sigma_o'^{m} \quad \text{.....2.1}$$

where V_p is the P-wave velocity, C_1 is a constant ($C_1 = V_p$ when $\sigma_o' = 1$ in the desired units), σ_o' is the isotropic confining pressure in the direction of wave propagation and **m** is .the slope on the log V_p - log σ_o' relationship. For the S-waves, this relationship is expressed as:

$$V_s = C_2 \sigma_o'^{n} \quad \text{.....2.2}$$

where V_s is the S-wave velocity, C_2 is a constant ($C_2 = V_s$ when $\sigma_o' = 1$ in the desired units), σ_o' is the isotropic confining pressure in the direction of wave propagation and n is .the slope on the log V_s - log σ_o' relationship.

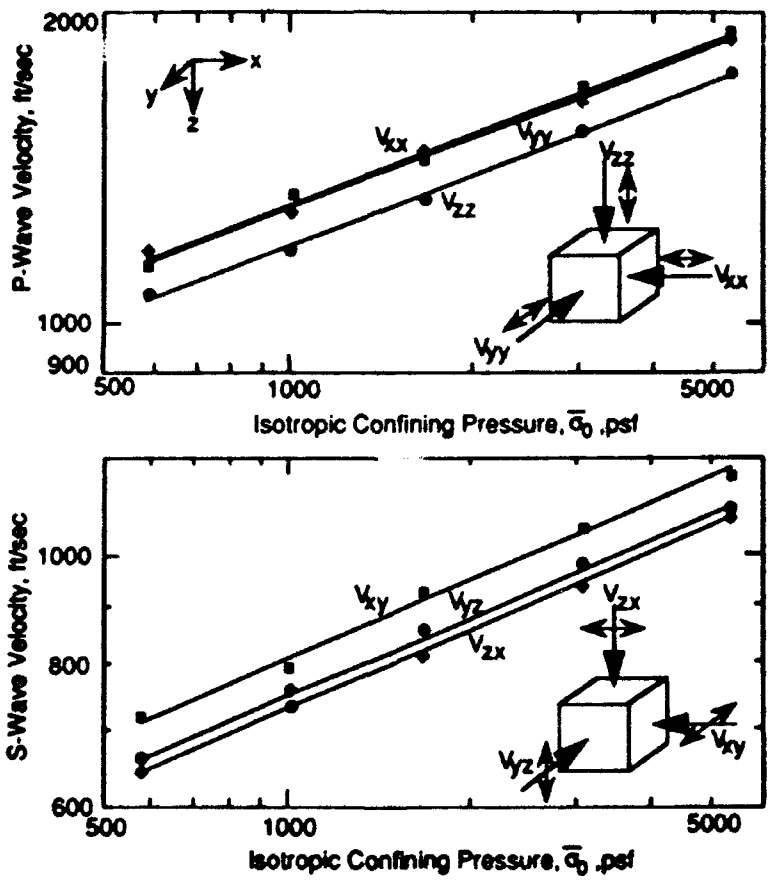

Figure 2.6: Variation of P- and S-Wave Velocities with Changes in the Isotropic Confining Pressure (Stokoe et al, 1991)

P-wave velocities are only affected by the stress in the direction of wave propagation for waves propagating along principle stress directions. This effect on wave velocity is shown in Figure 2.7 and can be expressed by the following equation:

$$V_p = C_1 \sigma_a'^{m} \quad \text{.....2.3}$$

where V_p is the P-wave velocity, C_1 is a constant, σ_a' is the effective principle stress in the direction of wave propagation and **m** is the slope on the log V_p - log σ_a' relationship.

Shear wave velocities are affected by the stresses in the directions of wave propagation and particle motion for waves propagating along polarized in principle stress directions. This effect on the wave velocity is shown in Figure 2.7 and can be expressed by the following equation:

$$V_s = C_2 \sigma_a'^{na} \sigma_b'^{nb} \quad \text{.....2.4}$$

where V_s is the S-wave velocity, C_2 is a constant, σ_a' is the effective principle stress in the direction of wave propagation, **na** is the slope on the log V_s - log σ_a' relationship, σ_b' is the effective principle stress in the direction of particle motion, and **nb** is the slope on the log V_s - log σ_b' relationship.

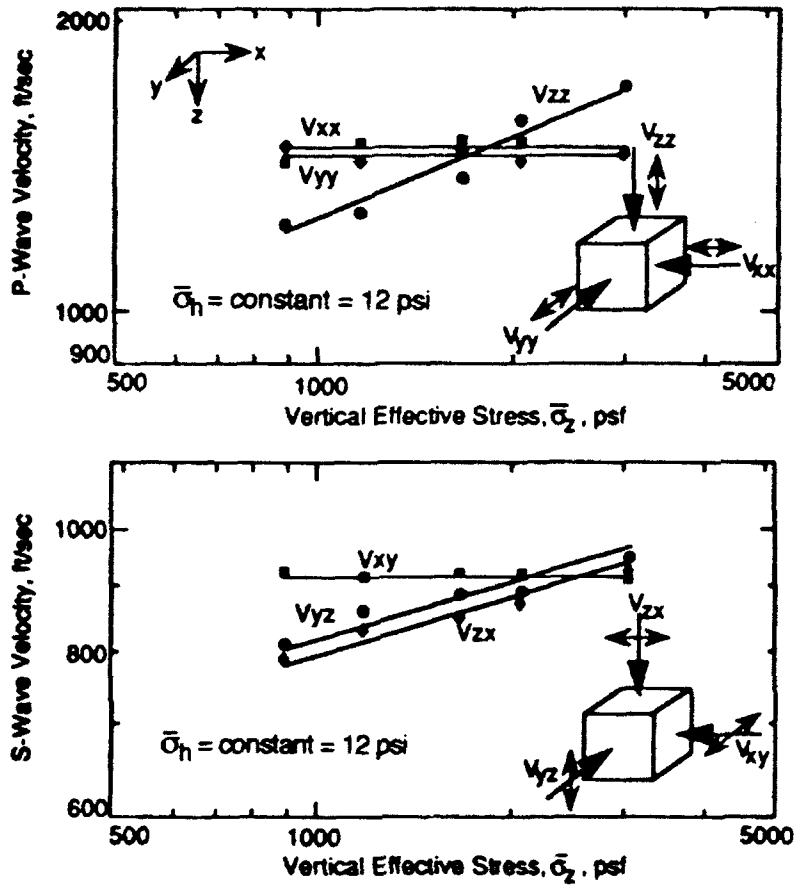

Figure 2.7: Variation of P- and S-Wave Velocities with Changes in the Vertical Effective Stress While the Horizontal Effective Stresses Remain Constant (Stokoe et al, 1991)

2.4 Use of Wave Velocities to Evaluate Soil Stiffness: The initial tangent modulus related to each wave velocity can be calculated by assuming an isotropic, homogeneous and elastic medium (Richart et al, 1970).

2.4.1 Shear Modulus: The shear modulus, G, is calculated using the shear wave velocity, V_s, and soil mass density, ρ, by:

$$G = \rho V_s^2 \quad \text{.....2.5}$$

where ρ is the total unit weight divided by the acceleration due to gravity.

2.4.2 Constrained Modulus: The constrained modulus, M, is calculated using the P-wave velocity, V_p, and the soil mass density, ρ, by:

$$M = \rho V_p^2 \quad \text{.....2.6}$$

2.4.3 Poisson's Ratio: Poisson's ratio, ν, is calculated using both the S-wave velocity and the P-wave velocity by:

$$\nu = [0.5(V_p/V_s)^2 - 1]/[(V_p/V_s)^2 - 1] \quad \text{.....2.7}$$

2.4.4 Modulus of Elasticity: The modulus of elasticity, E, is calculated using the S-wave velocity and Poisson's ratio:

$$E = 2\rho V_s^2 (1 + \nu) \quad \text{.....2.8}$$

or the P-wave velocity and Poisson's ratio:

$$E = 2\rho V_p^2 (1 + \nu)(1 - 2\nu)/(1 - \nu) \quad \text{.....2.9}$$

2.4.5 Resilient Modulus: Since there is no measurable permanent deformation during the seismic testing, the resilient modulus, M_R, is equated to the measured modulus of elasticity, E.

2.5 Effects of Overconsolidation and Plasticity Index: The stiffness of the soil subgrade is affected not only by the effective stress but also by the overconsolidation ratio (OCR) and the plasticity index (PI) of the soil subgrade (Hardin and Drnevich,1972). The shear modulus, G, increases with both PI and OCR as illustrated in Figure 2.8 and the following equation:

$$G_{max} = \frac{1230\ (2.973 - e)^2 (OCR)^k (\sigma_o')^{0.5}}{(1+e)} \quad \text{.....2.10}$$

where **e** is the void ratio, **k** is a function of PI as shown in Table 2.1, and σ_o' is the isotropic confining pressur in psi. In this equation, G_{max} is also in units of psi.

PI	K
0	0
20	0.18
40	0.30
60	0.41
80	0.48
>100	0.50

Table 2.1: Value of K as a Function of Plasticity Index (PI) (Hardin and Drnevich, 1972)

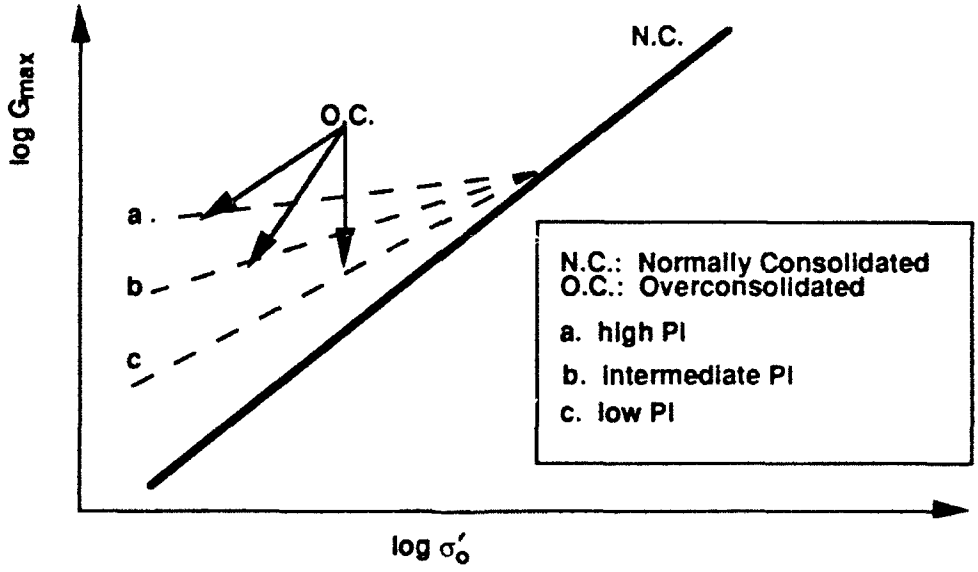

Figure 2.8: Effects of OCR and PI on the Shear Modulus

CHAPTER 3

EXPERIMENTAL DESIGN AND FIELD TESTING

The experimental procedures used in this study are explained in this chapter, which includes an in-depth description of the experimental design, equipment, and location, and the field testing procedures. This set-up could be used in practically any field condition.

3.1 Equipment: An array of twelve geophones (electromechanical devices which can transmit or receive vibrations within their calibrated frequency range and therefore can be used as both sources and receivers for the seismic waves; Stokoe et al, 1992) was used to measure the velocities of shear and constrained compression waves. The source signals were generated by a function generator which were in turn amplified by an audio amplifier and then sent to the source geophone. The received signals from the receiver geophones were recorded on a digital signal analyzer from which the arrival times of the waves were determined. All information generated by the digital signal analyzer was stored on magnetic disks. A tensiometer was used for evaluating negative pore water pressures in the soil subgrade and to correlate these values with the water content of the subgrade soil.

3.1.1 Geophones: The resonant frequency of the geophones used in this study was 60Hz. This frequency is much lower than the frequencies used in the field, which ranged from 1 - 5 KHz (the standard was 2 KHz). A proximeter was used to calibrate each geophone to determine the geophone's polarity with frequency. During calibration,

a black wire was connected to the positive terminal on each geophone. When the positive wire from the geophone was connected to the positive terminal of the digital signal analyzer, below 60 Hz an initial "up" source signal caused an initial "up" response from the geophone. Above 60 Hz, an initial "up" source signal caused an initial "down" response from the geophone (based upon the phase diagrams and direction of movement of the proximeter).

It is important to know the predicted direction of the initial arrival of the seismic wave signal in order to determine the travel time from the source geophone to the receiver geophone. When an S-wave is generated, some of the energy inherently generates a small P-wave, which often becomes coupled with the S-wave signal. Knowledge of the initial arrival direction of the S-wave signal greatly helps to differentiate between the two wave forms.

Each geophone is 1.25 in.(3.175 cm) in diameter, 1.40 in. (3.556 cm) long, and weighs 109 grams (see Figure 3.1). Installation of the geophones was a very sensitive step, since the orientation and precise distances between geophones are key factors in seismic testing (described in Section 3.1.1.3 and shown in Figures 3.8 and 3.9).

3.1.1.1 Assembly: The details associated with the assembly of the geophones were critical to ensure proper system response and longevity. Twenty five feet (7.6 m) of two-stranded cable with a foil shield and ground wire was attached to each geophone to ensure an adequate distance from the geophone to the recording point in the field after installation.

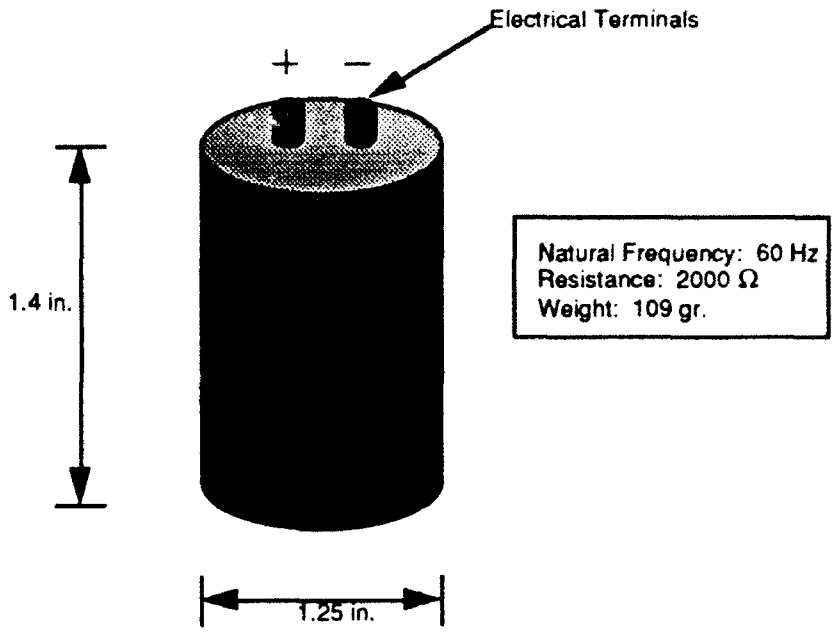

Figure 3.1: Geophone Characteristics

A geophone produces a differential output. As such, the geophone has two electrodes, positive and negative, to which corresponding positive and negative wires were soldered. (The colored wire was always soldered to the positive terminal and the black wire was always soldered to the negative terminal.) Care was taken to prevent the heat from the soldering iron from separating the interior soldered connections in the geophones. The geophones were placed in "Dixie" cups filled with a two-part epoxy (see Figure 3.2) to protect the geophones and wire from moisture infiltration once they were placed in the subgrade. In addition, silicon was used to seal the cable entry point into the epoxy. Each geophone has a piece of duct tape on the end of the cable with the geophone number written in large script for easy identification.

3.1.1.2 Calibration: The first step was to ensure that the geophones were still functional. Each geophone was individually connected to the digital

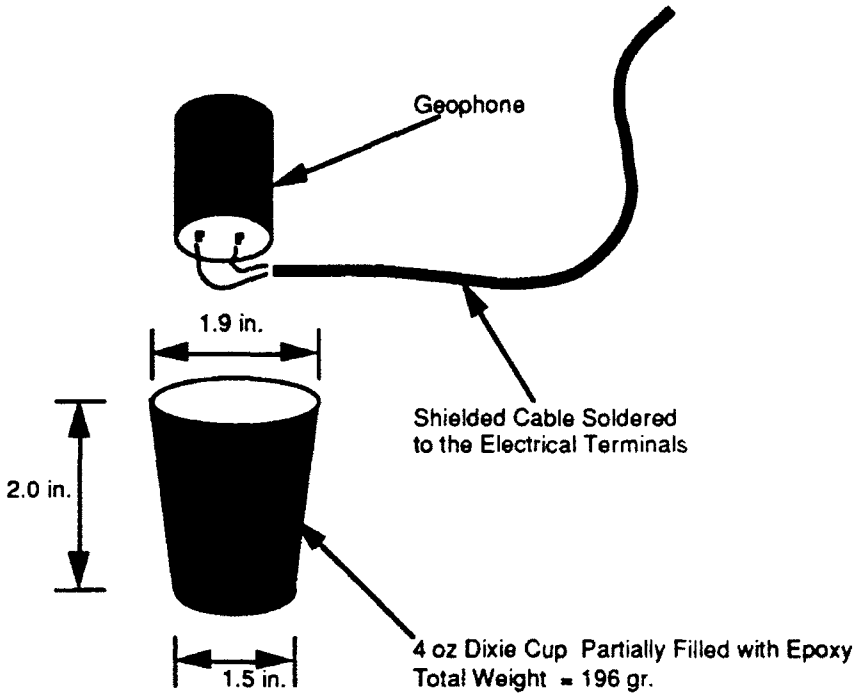

Figure 3.2: Geophone Assembly

signal analyzer and was used as a receiver to pick up any signals induced manually (a hammer blow on the floor, free vibrations, noise, etc.). Next, the geophone pairs (source and receiver) to be used in the field were calibrated in the laboratory to determine the time for the signals to travel through the equipment, wiring and geophones with no soil between the geophones.

Each pair of geophones was properly oriented relative to each other and then securely clamped together with hose clamps (see Figures 3.3 and 3.4). The geophones were then connected to the digital signal analyzer with a function generator and source amplifier connected to one of the geophones to provide a source signal (one cycle of a sine wave). The source geophone was used to generate a shear or constrained

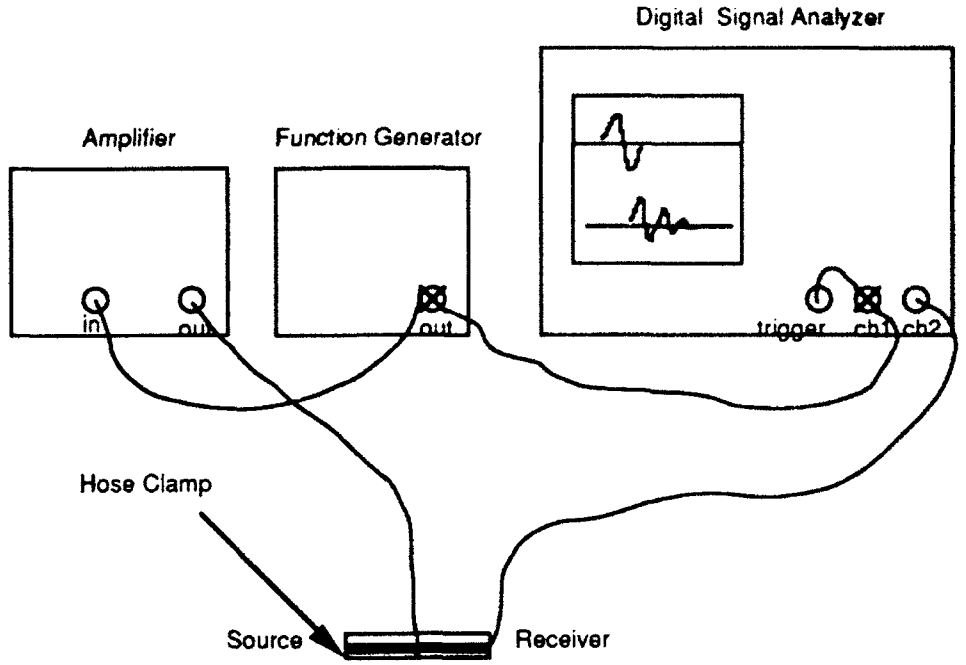

Figure 3.3: Schematic of Time-Delay Calibration for P-Wave Geophone Pairs

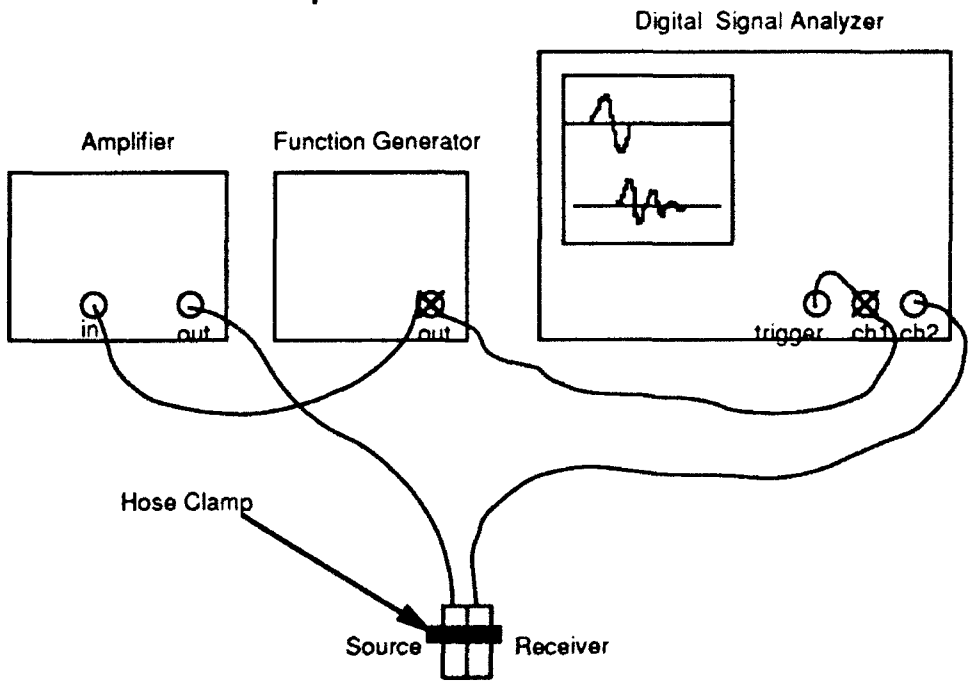

Figure 3.4: Schematic of Time-Delay Calibration for S-Wave Geophone Pairs

compression wave, depending upon its orientation. The receiver geophone was used to detect the seismic wave generated by the source geophone.

The difference in arrival times of the wave forms between the source geophone and the receiver geophone is the calibration factor. This factor is subtracted from the arrival times measured in the field because the times are between the source and receiver, just as measured in the calibration process, but with the source and receiver touching.

Because the arrival times varied with frequency and the frequency to be used in the field may vary, the geophone sources were driven with a frequency swept signal to compare the phase angle with frequency, as illustrated for the P-wave geophone pair 8/9 in Figure 3.5. The records for the other geophone pairs are presented in Appendix B. *The time delay, t, then is a function of the phase angle, ϕ, and frequency, f, by:*

$$t = \phi / (360 \times f) \quad \text{.....3.1}$$

For shear and compression wave measurements, the time delays varied as shown in Table 3.1.

Wave Type	Geophone Pair	Arrival Time Correction (ms)
P	8-9	0.093
SH	7-8	0.172
SH	11-12	0.206
SV	13-14	0.150
SH	2-5	0.092
P	1-17	0.076

Table 3.1: Arrival Time Corrections for Different Geophone Pairs

resistance measured in the field differed by more than 0.100 KΩ, it was assumed that moisture had gotten into the system and the geophone measurements were adversely affected.

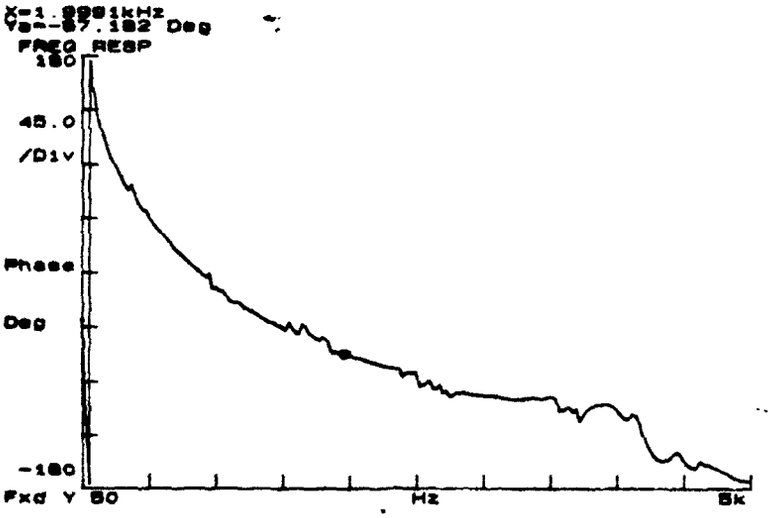

Figure 3.5: Typical Calibration Curve Showing a Time-Delay Represented by the Phase for Geophone Pair 8/9

Geophone	Geophone Resistances (KΩ) Dates of Measurement				
Number	Lab	18-Jul	10-Aug	11-Aug	12-Aug
1	2.040	2.129	2.061	2.076	2.102
2	2.010	2.095	2.037	2.062	2.042
5	2.010	2.116	2.103	2.100	2.007
7	1.990	2.089	2.004	2.009	2.033
8	2.010	2.099	2.014	2.028	2.011
9	2.020	2.103	2.100	2.101	2.099
10	2.030	0.002	0.002	0.002	0.002
11	2.020	2.112	2.058	2.009	2.116
12	2.030	2.123	2.113	2.115	2.098
13	2.010	2.099	2.055	2.087	2.048
14	2.010	2.106	2.076	2.090	2.101
17	2.020	2.133	2.111	2.140	2.103

Table 3.2: Geophone Resistances for Each Test Day

3.1.1.3 Installation: Each pair of geophones was placed in the field on 20 June 1992 in particular orientations to measure the velocity of the corresponding wave type. Using a small, gasoline engine auger (see Figure 3.6), four holes were bored to 18 in. (46 cm) below grade. After carefully removing excess soil and measuring the depth, each geophone was placed in the proper hole as depicted in Figure 3.7. All the geophones were placed at a depth of 18 in. (46 cm) below grade except geophones 5 and 17, which were placed at a depth of approximately 8 in. (20 cm). Each pair of geophones was properly oriented, with the geophones approximately one foot (0.3 m) apart. The final configuration involving 12 geophones is shown in Figure 3.8. The individual pairs of geophones, types of waves measured, distances apart and direction of measurement are listed in Table 3.3. Two plumb bobs were used to accurately locate each geophone pair's position horizontally in reference to each other, as illustrated in Figure 3.9. Soil was carefully placed back around each geophone and compacted in an attempt to achieve the same density as the surrounding compacted fill. The geophone cables were placed in a small trench leading out to the edge of where the pavement would be placed.

Later that day, one of two 6 in. (15 cm) lifts of type "A" asphalt was placed over the site and compacted with a vibratory roller. The second lift was placed the following day. One 3 in. (10 cm) lift of type "B" asphalt and a 2 in. (5 cm) lift of type "C" asphalt were placed on subsequent days for a total of 17 in. (43 cm) of asphalt pavement overlying the soil subgrade.

Geophone Pair	Wave Type	Distance Apart*	Direction of Measurement
8-9	P	1.45 ft.	E-W
7-8	SH	1.27 ft.	N-S
11-12	SH	1.31 ft.	E-W
13-14	SV	1.29 ft	E-W
2-5	SH	0.72 ft.	Vertical
1-17	P	0.79 ft	Vertical

* Near-edge to near-edge

Table 3.3: Listing of Wave Types, Distances and Directions of Geophone Pairs

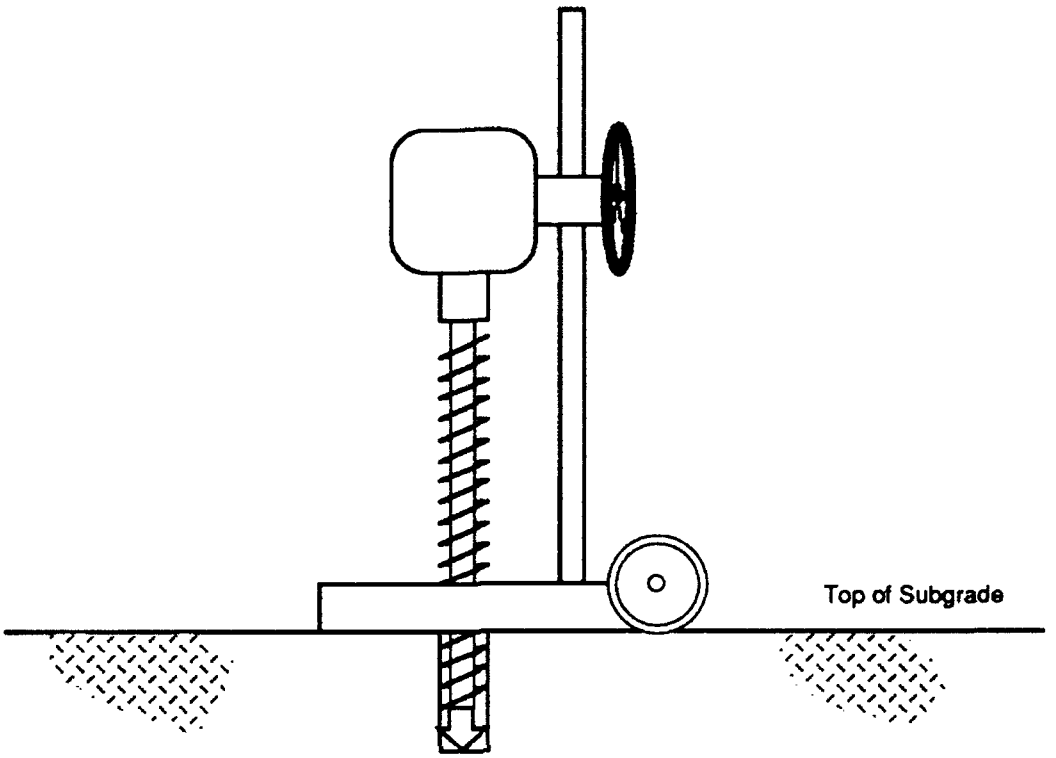

Figure 3.6: Borehole Augering Operation

3.1.2 Signal Generation: The electrical signal sent to the source geophones was one cycle of a sine wave at a frequency of 2 KHz from a function generator. The 5-volt signal was amplified by a factor of 15 to 20 before being sent to the geophones. The signal was also sent to channel 1 of the digital signal analyzer to trigger the source wave. The signals received by the geophones were recorded and displayed on the digital signal analyzer with 50 averages typically taken. The averaged signals were saved on 3.5 in. (8.9 cm) magnetic disks. The equipment used in the signal processing is described in the following sections.

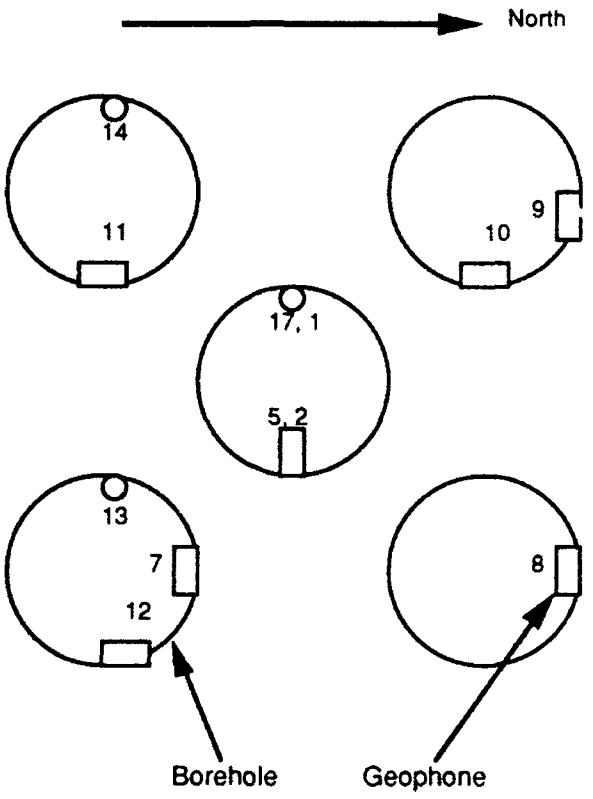

Figure 3.7: Plan View of Geophone Orientations in Boreholes

3.1.2.1 Function Generator: The function generator used to send an electrical signal to the source geophone was a Model 3314A by Hewlett-Packard. It is a multi-mode, programmable function generator which features sine, triangle and square wave functions from 1 mHz to 19.99 MHz. The operating modes include Free Run, Gate and N Cycles. In addition, the function generator has a programmable time interval for

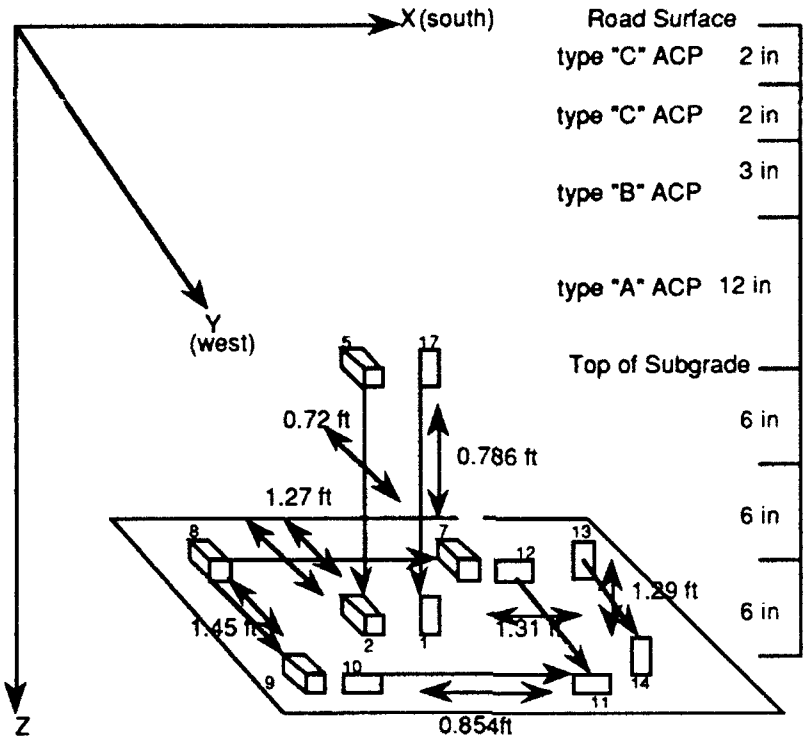

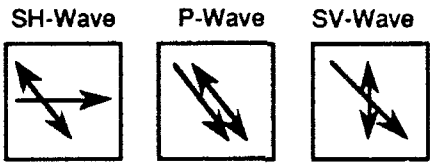

Notes: Traffic is in the Y direction.
All distances between geophones are near- edge to near-edge.
Black wire is connected to the positive geophone terminal.
Above 60Hz, positive geophone wire connected to a positive connection on the digital analyzer yields an " up " signal.
Geophone # 10 was damaged during testing and is no longer functional.
Distances in the diagonal directions are unknown.

Figure 3.8: Layout of 12 Geophones Placed in the Subgrade

internal triggering. The function generator was programmed for all seismic tests in this study to send one cycle of a 5-volt, 2 KHz sine wave every 100 msec to the source geophone.

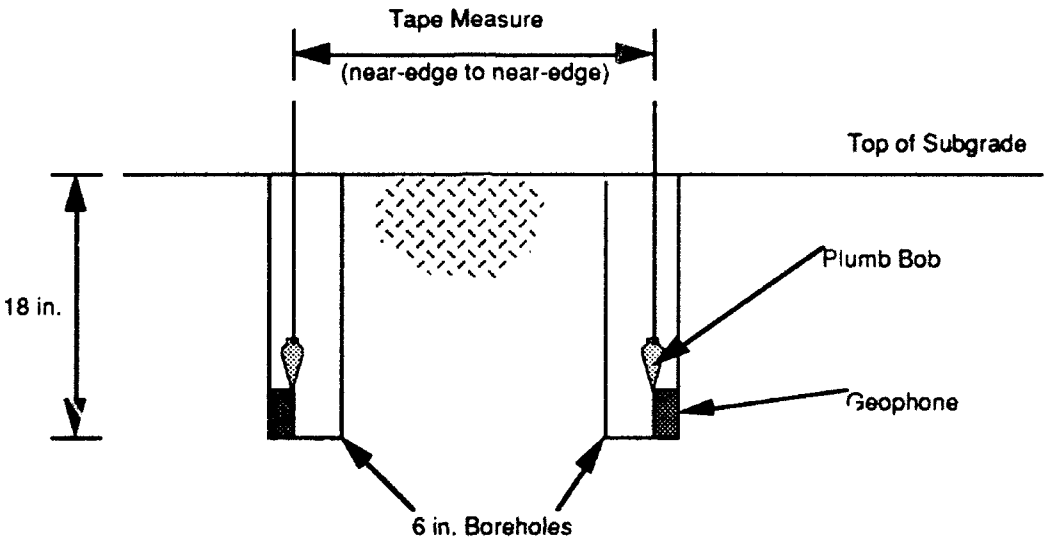

Figure 3.9: Geophone Installation

3.1.2.2 Amplifier: The amplifier used was a Model SS530 audio range amplifier by MB Dynamics, for voltages up through 200V. The amplifier boosted the 5 volt signal from the function generator to between 75 and 100 volts.

3.1.2.3 Digital Signal Analyzer: The digital signal analyzer used was a Hewlett-Packard 3562A Dynamic Signal Analyzer. It is a completely programmable signal processor with the capability of analyzing the frequency, amplitude, phase or any mathematical function of those. It has programmable internal triggers and sources, and it can also be set to accept external triggers or external sources. The analyzer has two input/output channels and one external trigger channel. The sources can be band

limited, band translated random noise, burst random, sine chirp, burst chirp, as well as fixed sine and swept sine signals. The trigger can be free run, input from channel 1 or 2, source, or externally triggered.

The analyzer was programmed for the seismic testing to accept a source signal from the function generator on channel 1 with a sensitivity range of 10 volts and the receiver signal on channel 2 with a sensitivity range of 4 millivolts. The analyzer triggered off channel 1 at a level of 2 volts with a delay of 200 milliseconds. The number of averages was set to 50. An important function was the overrange reject, which when turned off, would allow a small (relative to the ambient noise) signal received on channel 2 to be detectable.

3.1.2.4 Disk Drive: The disk drive was a Hewlett-Packard 9122, with two disk drives. It was used to store all data from the digital analyzer on 3.5 in. (8.9 cm) high-density magnetic disks.

3.1.3 Multimeter: A multimeter, Model Micronta by Radio Shack, was used to measure the resistances of the geophones.

3.1.4 Wheel-Load Scale: A wheel-load scale was used for determining the wheel loads on the pavement for the stress analysis. The scale was borrowed from the Texas Department of Public Safety from Sgt. Cummings of the License and Weight Division. The scale was Model DT300 made by Intercomp and had a range of 20,000 lbs.(89 KN) in the 50-lb.(222 N) increment mode.

3.1.5 Tensiometer: Tensiometers (Stannard, 1990) measure soil "suction" or, more precisely, negative pore water pressures. The device used in the study was an 18-in. (45.7 cm) long tensiometer made by Irrometer. It is simply composed of a porous cup connected to the bottom of a clear plastic tube with a gage attached as shown in Figure 3.10. The porous cup is saturated with water, and the tube is filled with water.

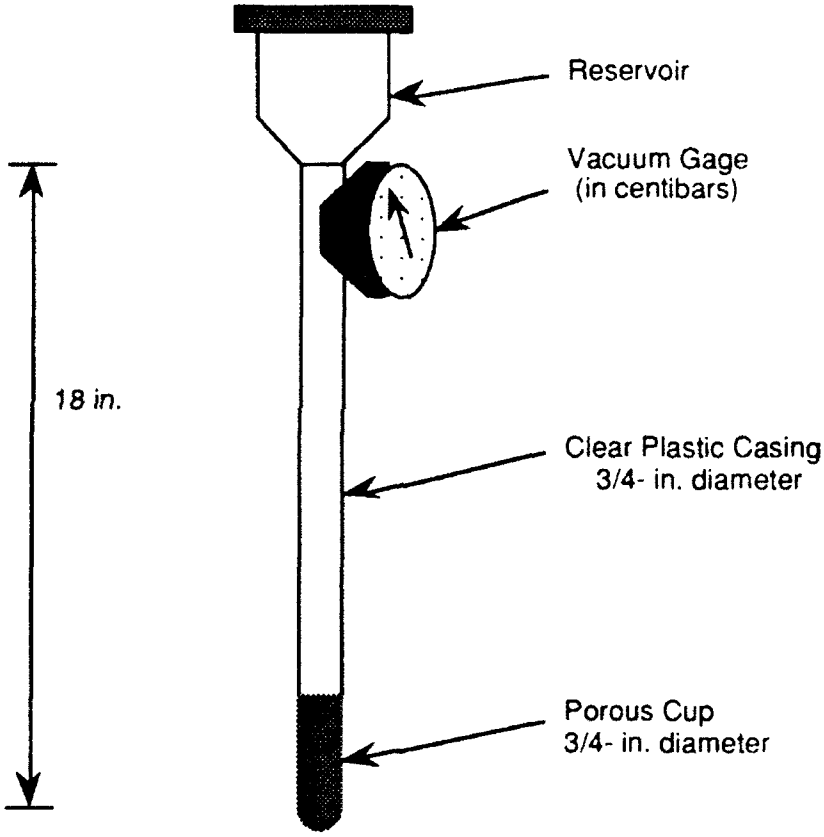

Figure 3.10: Tensiometer

In the same general vicinity as the geophones, a 4-inch (10 cm) diameter hole was bored through the asphalt and into the soil using an electric coring rig (see Figure

3.11). The hole penetrated 6 inches (15 cm) into the soil and was cased with a 4-inch (10 cm) diameter stainless steel pipe. A removable rubber cap seals the hole from invading water, and a six- inch (15 cm) square plate protects the top of the casing from vehicular damage. A hole about the size of the diameter of the porous cup is made in the soil, and the tensiometer is inserted into the hole. After equilibration (when the negative pore pressures are not changing significantly - which takes approximately one hour), the negative pore water pressure can be read from the gage. The water content can be determined from a correlation with the negative pore water pressure (see discussion under Section 3.2.2).

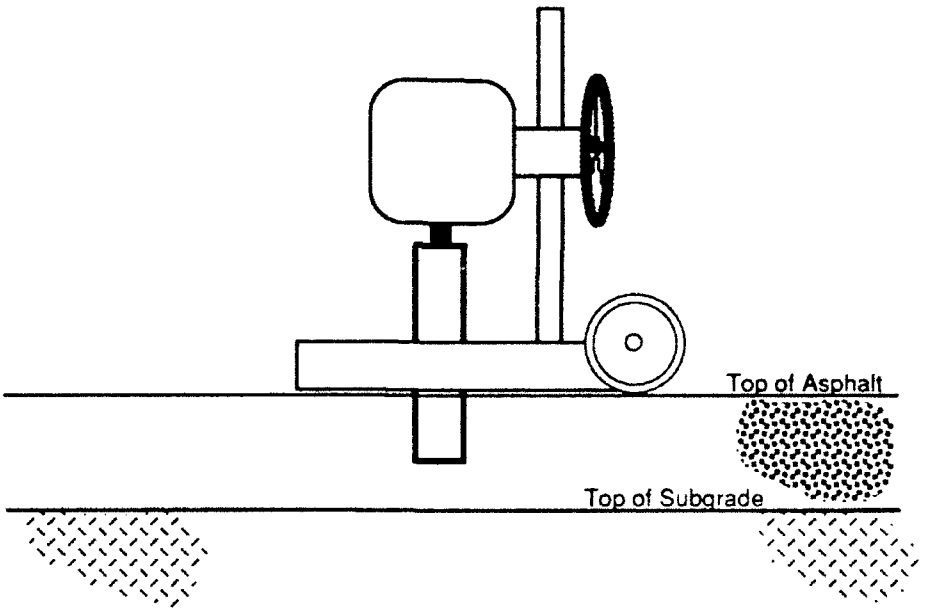

Figure 3.11: Electric Coring Rig for Tensiometer Installation

3.2 Pavement Material Properties: Several pavement material properties were required for analyzing the data collected from the digital signal analyzer to calculate the appropriate soil moduli: soil unit weight, Atterberg limits, water content and negative pore water pressure, and the asphalt modulus of elasticity. These properties and the associated procedures for obtaining them are discussed in the following paragraphs.

3.2.1 Soil Sampling: Relatively undisturbed samples of the compacted fill material were obtained on 20 June 1992 by pushing three-inch (7.6 cm) diameter Shelby tubes into the ground. The "pushing" was difficult due to the high degree of compaction achieved and the low water content. By jacking up the front end of the soil dynamics van and lowering it onto the Shelby tubes, the tubes were forced into the ground as illustrated in Figure 3.12. Several jacking procedures were necessary to push each tube at least 18 inches (46 cm) into the ground. When two representative samples were obtained, the ends of the tubes were sealed with hot wax and transported to the laboratory to be stored in the wet room for future use.

3.2.2 Soil Unit Weight: The dry unit weight of the soil was determined by carefully cutting one of the two Shelby tubes to a convenient length (about 4 in./10 cm) with a representative sample of soil. The ends of the soil in the tube were carefully trimmed perpendicular to the length of the tube. The tube was weighed with the soil in it (1173g) and then dried in the oven for 2 days. After weighing the soil and tube in the dry state (1033g), the soil was extruded to weigh the empty tube for the tare weight (308g). The dimensions of the tube were measured to be 4.2 in. (10.7 cm) in length and 2.87 in. (7.3 cm) for the inside diameter. With the volume of the tube and the dry weight of the soil, the dry unit weight of the in-situ soil was determined be 101.6 pcf (1619 kg/m^3). The in situ total unit weight was 121.2 pcf (1931 kg/m^3) with a water content of 19.3 %. Assuming a specific gravity of 2.7, the void ratio, e, was calculated to be 0.66.

3.2.3 Water Content: From one of the two field samples obtained, a sample was taken for determining the water content. The wet soil was weighed, oven dried and weighed again. The weight of the water, divided by the weight of the dry soil, is the water content (in percent when multiplied by 100%).

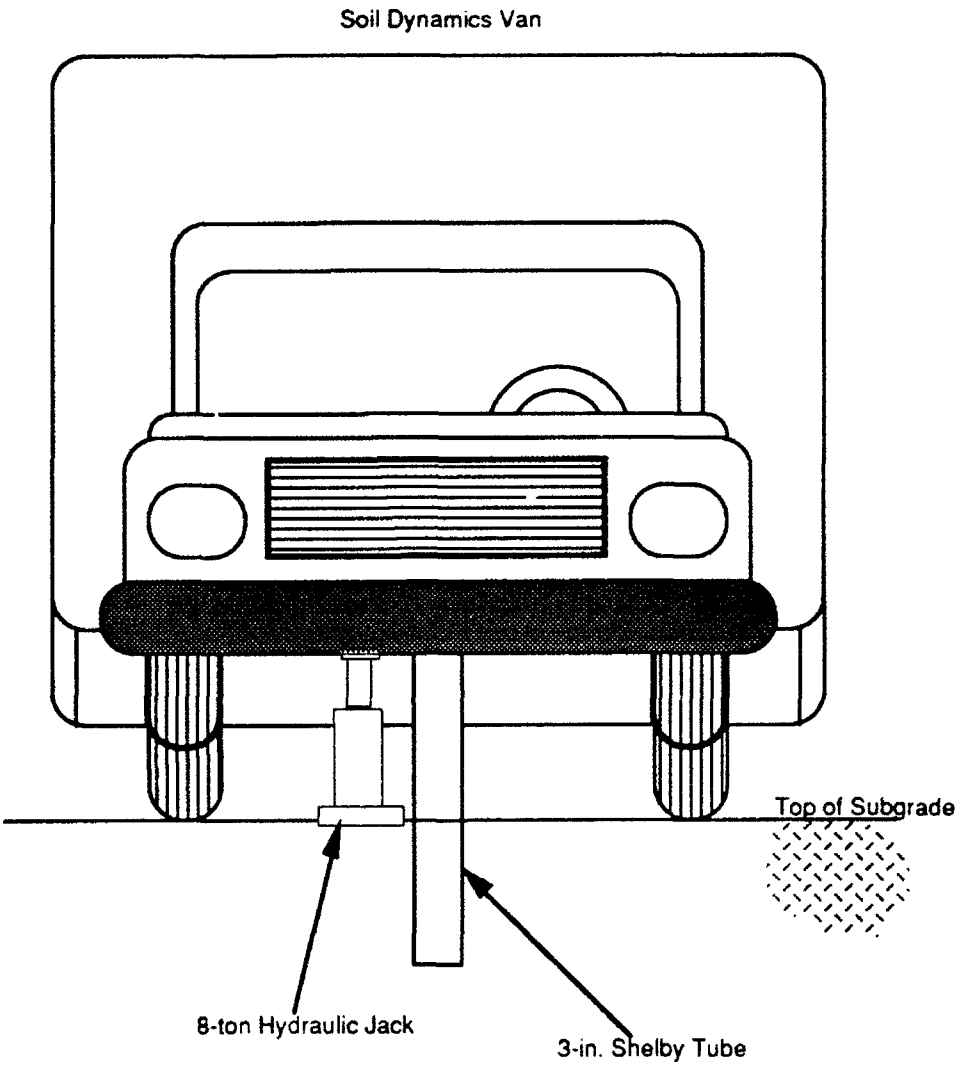

Figure 3.12: Soil Sampling Technique

The in situ water content was determined through correlations with negative pore pressures obtained with a tensiometer. Using an undisturbed soil sample (left in the Shelby tube), a probe of the same diameter as the tensiometer was inserted into the top 2 in. (5 cm) of the soil. Carefully ensuring good contact with the soil, the tensiometer was

inserted into the hole. After allowing the soil and tensiometer to equilibrate (approximately 30 min. to 1 hr.), the negative pore water pressure was read off the gage. Immediately a portion of the tested soil was taken to determine the water content for that pore water pressure.

The water content found in the field sample (19.3 %) and the corresponding water content found with the negative pore water pressures of the field measurements (15 centibars) were the same; therefore a correlation curve was not required. Had it been necessary to perform this operation, the following procedures would have been followed. Water would have been added to the sample and left overnight to equilibrate. The process of testing the negative pore water pressure and finding the water content would have been repeated 4 to 5 times for the wetting curve. The drying curve would also be determined by the same process except that the soil would be allowed to dry overnight for each correlation. When the in situ pore water pressures are measured over long periods of time, it is important to know whether or not the soil is in a wetting or drying process (usually in the summer it is a drying process and in the winter a wetting process). Therefore, tensiometer readings are taken each testing day in the field.

3.2.4 Atterberg Limits: The Atterberg limits were obtained for one soil sample following ASTM standard D4318-84. The liquid limit was found to be 32 % and the plastic limit was 17 %.

3.2.5 Asphalt Modulus of Elasticity (by SASW Method): The modulus of elasticity of the asphalt surface layer was required for calculating the vertical stress induced in the soil at the depth of the geophones by a surface load on the pavement. The Spectral-Analysis-of- Surface-Waves (SASW) technique was used to

evaluate the modulus. The SASW testing process is illustrated in Figures 3.13 through 3.21. The pavement was tested on 20 August 1992 and cross-power spectra plots were recorded. The analysis and figures are presented in Chapter 4.

As shown in Figures 3.13 -3.21, surface waves were generated using a hammer or a Piezoelectric shaker (Model F-7 by MB Dynamics) as the source. A small ballpeen hammer generated waves with short wavelengths for spacings of 6 in. (15.24 cm) to 2 ft. (60.96 cm). A masonry hammer generated waves with longer wavelengths for the spacing of 4 ft. (121.92 cm). The sledge hammer generated waves for the longest spacings of 12 ft. (3.66 m) and 16 ft. (4.88 m). The F-7 shaker produced waves over a wide range of frequencies at the spacings of 6 in. (15.24 cm), 1 ft. (0.3 m), 2 ft. (0.6 m) and 4 ft. (1.2 m). Two different receivers types were used to detect the surface waves; Wilcoxon 736 accelerometers for wavelengths up through 4 ft. (121.92 cm), and 1-Hz geophones for wavelengths in excess of 4 ft. (121.92 cm). The accelerometers were coupled with the asphalt by hammering nails with large flat heads into the asphalt surface. The nails were spaced at 6 in. (15.24 cm), 1 ft. (30.48 cm), 2 ft. (60.96) and 4 ft. (121.92 cm). Magnets were used to attach the accelerometers to the nail heads. The 1-Hz geophones were coupled to the asphalt by placing high vacuum grease on the bottom of the geophone and pressing the geophone onto the pavement surface.

By varying the distance that the two accelerometers (or geophones) were apart, waves of different wavelengths could be measured traveling between the accelerometers(or geophones). With accelerometers at shorter distances apart, the waves sampled the more shallow depths into the surface layer.

At longer distances apart, 1-Hz geophones were used, which were able to receive

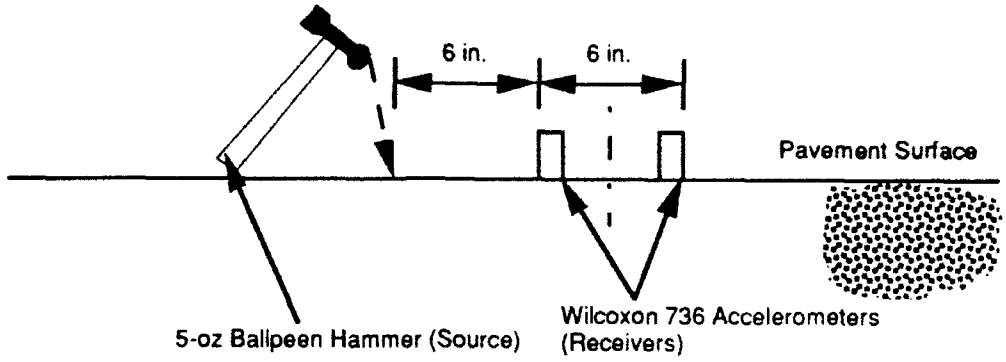

Figure 3.13: SASW Testing at 6-in. Spacing with Small Hammer Source

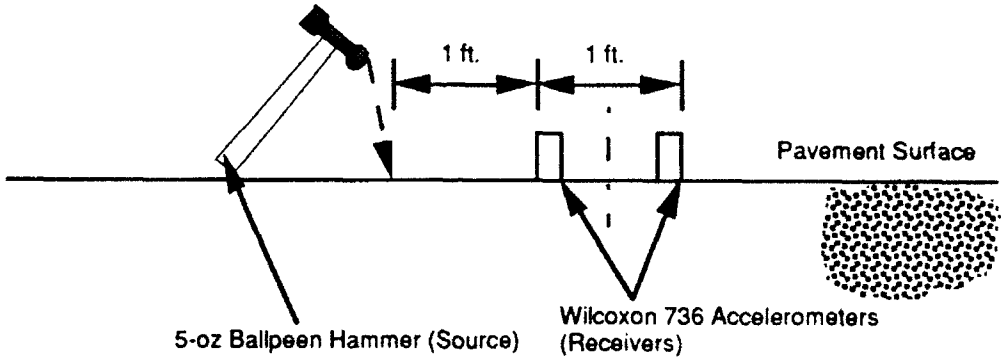

Figure 3.14: SASW Testing at 1-ft. Spacing with Small Hammer Source

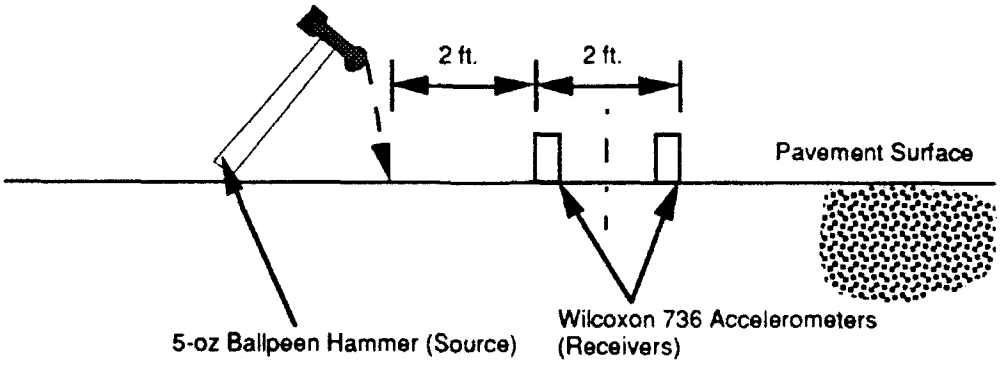

Figure 3.15: SASW Testing at 2-ft. Spacing with Small Hammer Source

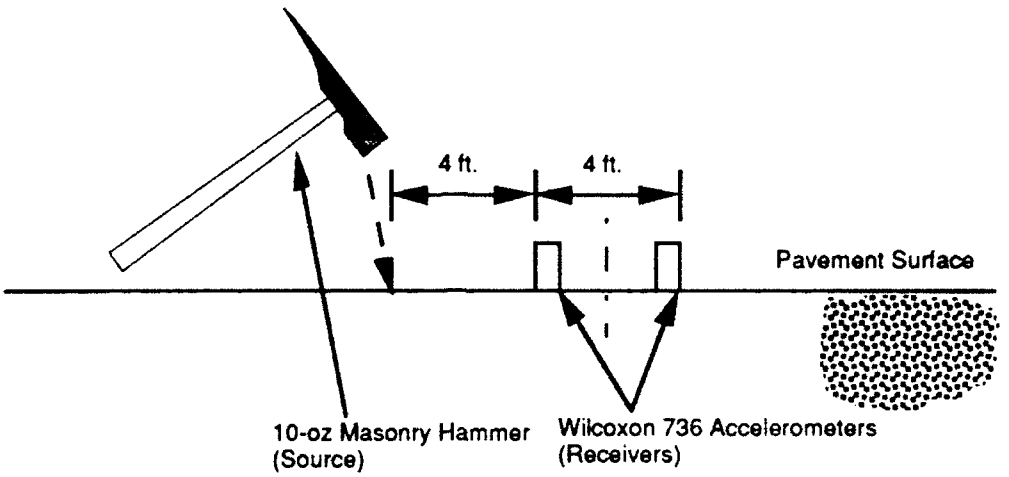

Figure 3.16: SASW Testing at 4-ft. Spacing with Medium Hammer Source

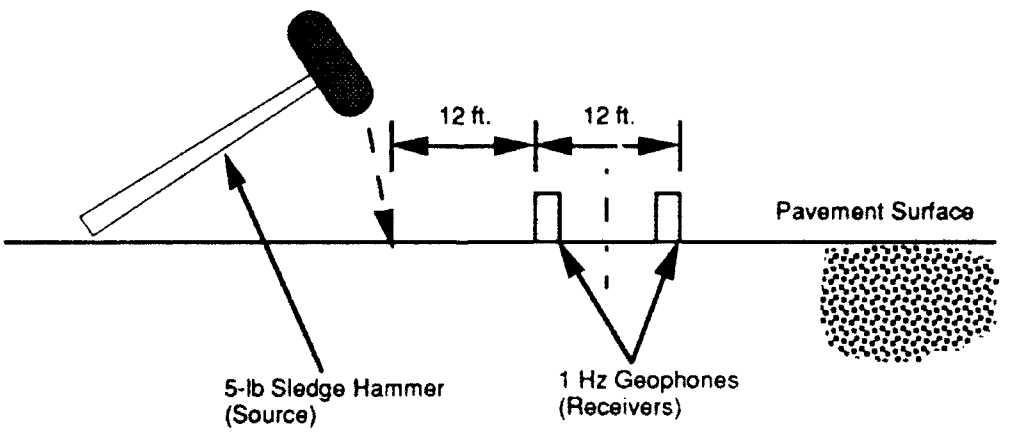

Figure 3.17: SASW Testing at 12-ft. Spacing with Large Hammer Source

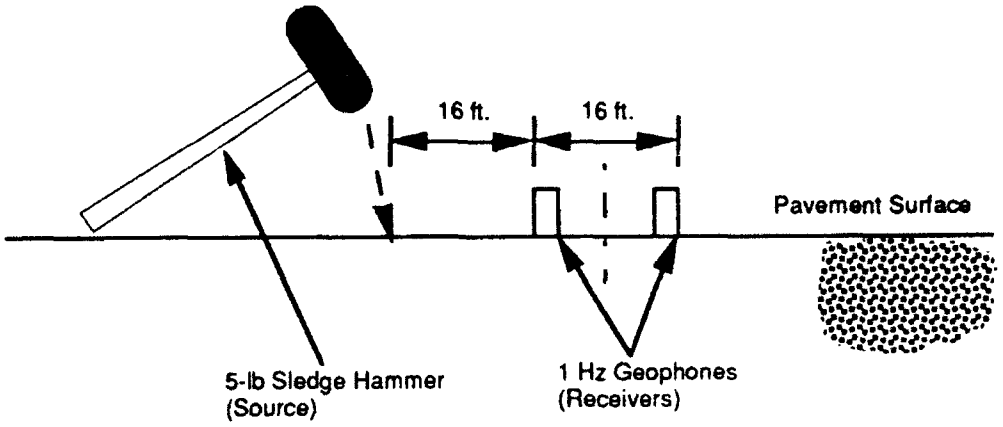

Figure 3.18: SASW Testing at 16-ft. Spacing with Large Hammer Source

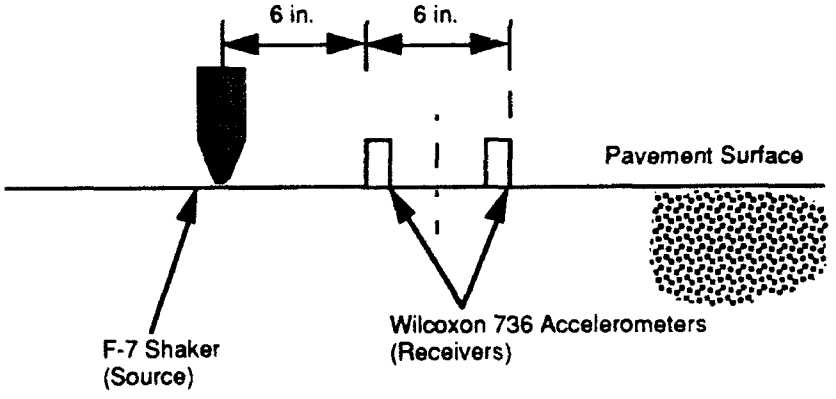

Figure 3.19: SASW Testing at 6-In. Spacing with F-7 Shaker Source

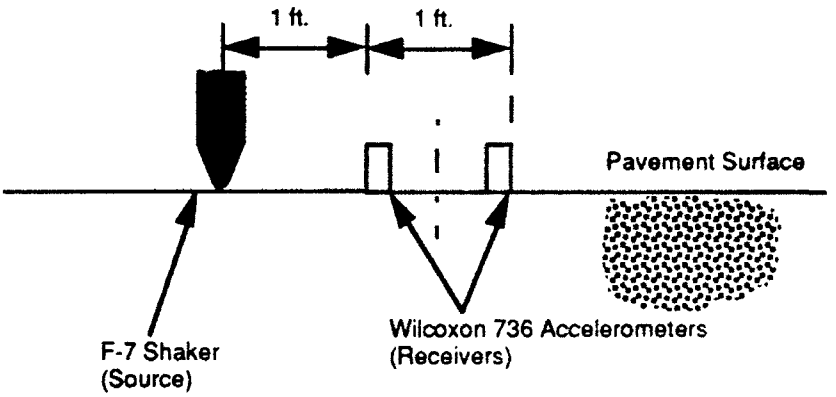

Figure 3.20: SASW Testing at 1-ft. Spacing with F-7 Shaker Source

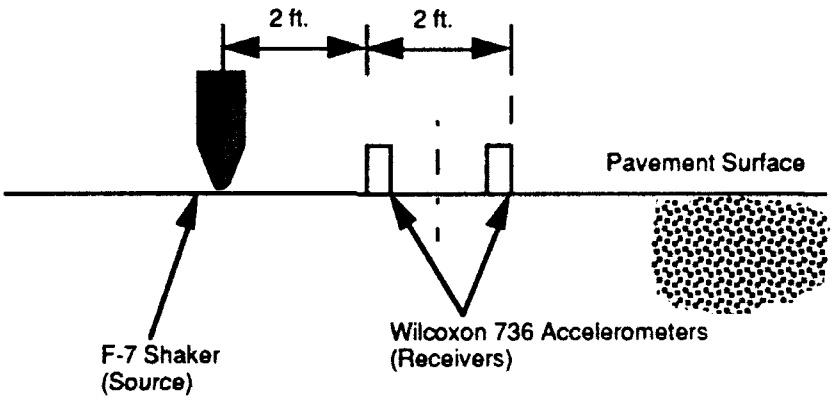

Figure 3.21: SASW Testing at 2-ft. Spacing with F-7 Shaker Source

waves at the lower frequencies (longer wavelengths). Using surface waves of different wavelengths, the variation of wave velocity with wavelength (dispersion) was obtained (Aouad et al, 1992).

A digital signal analyzer (Model HP 3562A) was used to capture, store and process the receiver outputs. This analyzer is capable of calculating Fast Fourier Transforms on recorded data in real time which is a critical requirement for allowing the operator to immediately access the quality of the data being processed, and, if necessary, modify the arrangement of source and receivers or other test parameters accordingly (Stokoe et al, 1989).

3.3 Site Description: For future reference and study, it is important to know the location of the test site.

3.3.1 Location in Austin, TX: One site was tested in this study. The test site is located approximately one-half mile (0.8 Km) west of Interstate 35 on US Route 183 at Gessner Lane (see Figure 3.22).

3.3.2 Location of Test Equipment at the Site: The test equipment is buried under the pavement of Gessner Lane between the northbound and southbound lanes of US Highway 183. This location is shown in Figure 3.23. The test equipment can be found by first locating three brass screws in the top of the curb on the east side of Gessner, approximately 30 ft. (9 m) from the westbound lane of Highway 183.

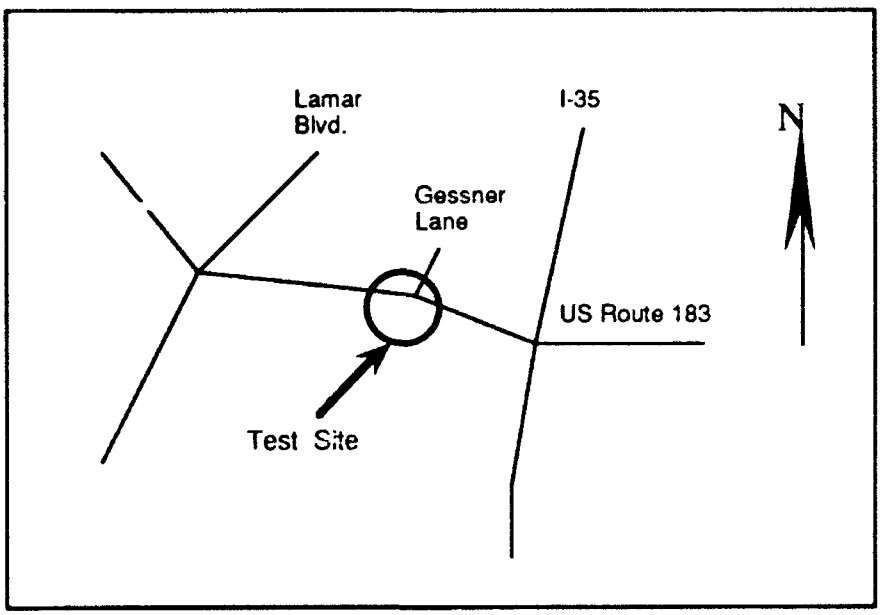

Figure 3.22: Location of Test Site on Gessner Lane in Austin, Texas

Permanent markers were installed on top of the curb to aid in locating the tops of the tensiometer casing, geophone array and cable manhole. Three small brass screws were installed by drilling three 1/8 -in. (3 mm) diameter holes on top of the curb with a drill and masonry drill bit, and then filling the holes with a permanent epoxy. The brass screws are flush with the top of the curb. The tops of the tensiometer casing, geophone array and cable manhole are located by measuring from the brass screws and finding where the arcs intersect as illustrated in Figure 3.24. The steel plate covering the cable manhole has been buried under approximately 18 in. (46 cm) of top soil, as depicted in Figure 3.25. The remaining two-inch (5 cm) lift of asphalt will bury the steel plate covering the tensiometer casing. The tensiometer was not left in the ground, but must be reinserted for future testing.

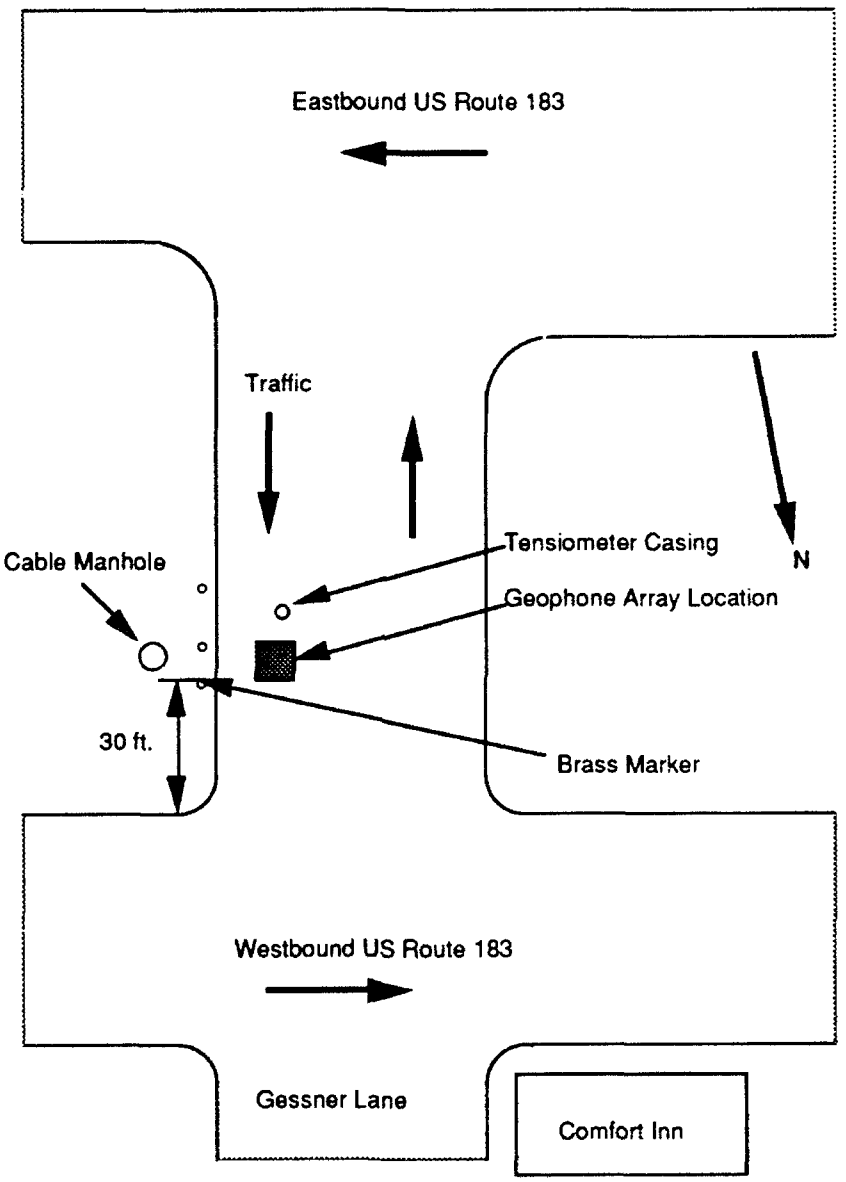

Figure 3.23: Site Plan of Testing Area

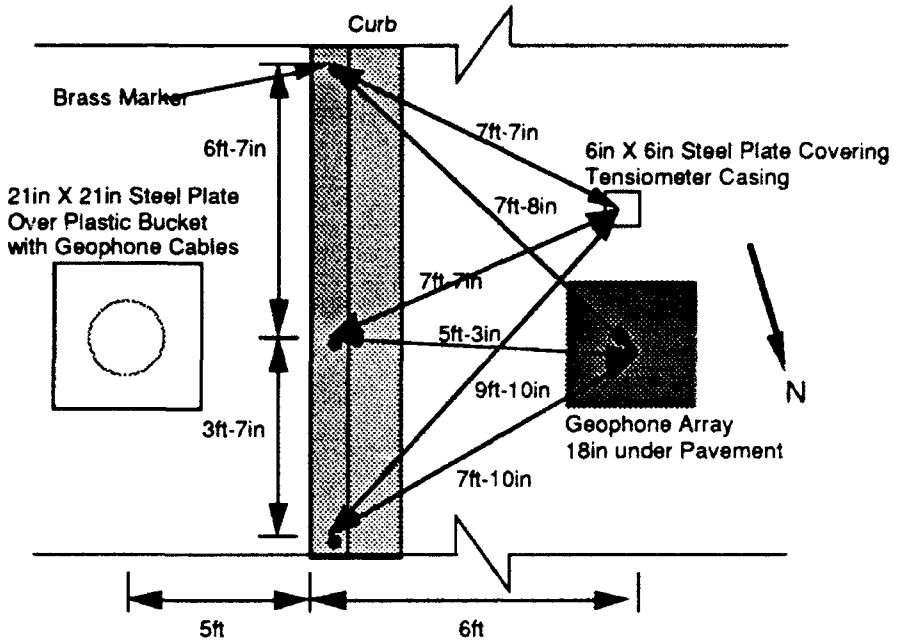

Figure 3.24: Plan View of Test Site

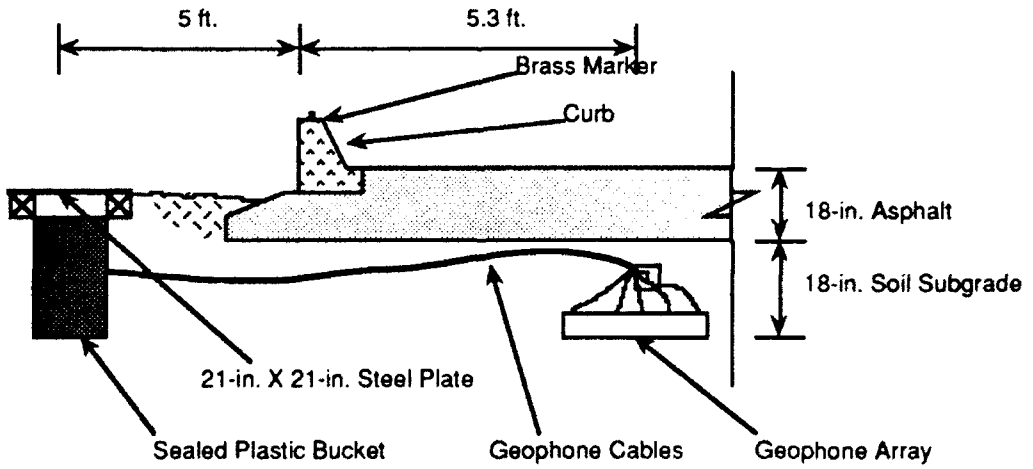

Figure 3.25: Cross-Section of Test Site

3.4 Seismic Testing Procedures: Specific procedures were followed each testing day (18 July, 10 - 12 August 1992). First, the water content was determined using the tensiometer and the correlation between the negative pore water pressures and the water contents obtained in the laboratory (15 centibars and 19 %, respectively because no difference was ever measured). The resistivities of the geophones were determined with an ohmmeter and checked against the baseline values established in the laboratory (see Section 3.1.1.2). The only discrepancy found was that geophone number 10 had been damaged (the resistance measured was 0.002KΩ vs. the 2.028 KΩ found in the laboratory). Unfortunately, a large direct current was inadvertently used in driving this geophone which caused the coil to burn up (therefore causing the resistance to decrease).

The location of the geophone array was found as described in Section 3.3.2. To perform each seismic measurement, the desired geophone pair was first selected. The geophone pair was then connected to the digital signal analyzer and source amplifier (the colored wire was always connected to the positive terminal and the black wire was always connected to the negative terminal on the equipment to ensure that an "up" source signal produced an initial "up" response on the receiver geophone). The electrical signal sent from the function generator through the amplifier excited the source geophone. Simultaneously, the function generator sent a trigger signal to the digital signal analyzer. The trigger signal and the arrival of the seismic wave through the soil at the receiver geophone were recorded on the digital signal analyzer as shown in Figure 3.26.

The first arrival of the wave form was recorded in the time domain and averaged with subsequent signals. A standard number of averages used was fifty. Typical P-wave and S-wave time records are shown in Figures 3.27 and 3.28, respectively. In addition,

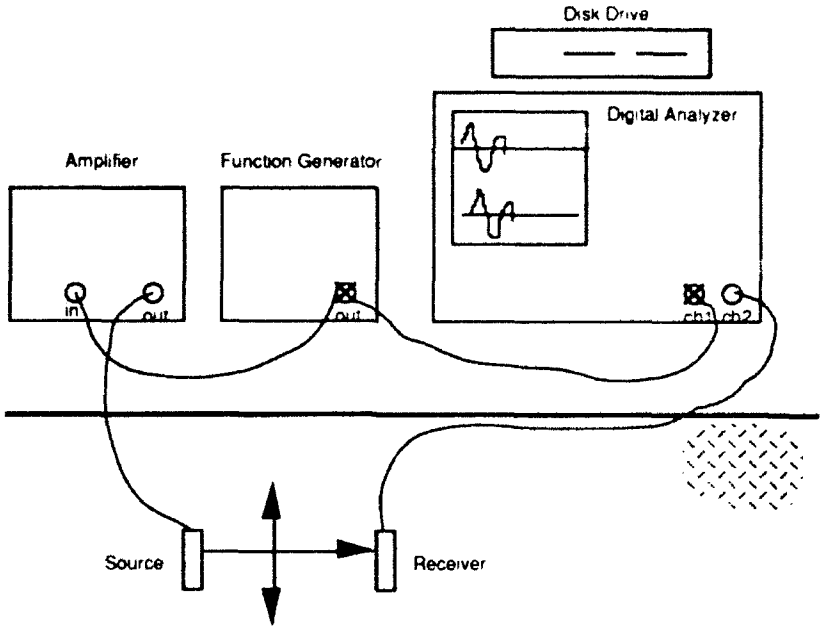

Figure 3.26: Equipment Set-up for Seismic Testing

the time records from the seismic testing conducted on 12 Aug. 1992 for all the geophone pairs tested with an added surface load of 10,200 lbs (45.4 KN) are included in Appendix A. The vertical marker on the top left side of each time record indicates the time at which the source signal began. The vertical marker on the bottom right side of each time record indicates the time at which the respective wave form initially arrived at the receiver geophone.

The source and receiver geophone wires were switched and the process was repeated. These two averaged first arrival times were also averaged together and used with the geophone spacing and calibration factor (for a 2 KHz signal) to obtain the particular wave velocity. This procedure was repeated for the other geophone configurations to determine the anisotropy of the soil formation with no induced overburden stress (see analysis and tables in Chapter 4). A typical set of data is given in Table 3.4.

Wave Type	Geophone	Wave Velocity (fps)
P	8-9	1203
SH	7-8	632
SH	11-12	569
SV	13-14	565
SH	2-5	545
P	1-17	1301

Table 3.4: Wave Velocities from Seismic Testing on 10 Aug. 1992 with No Added Surface Load

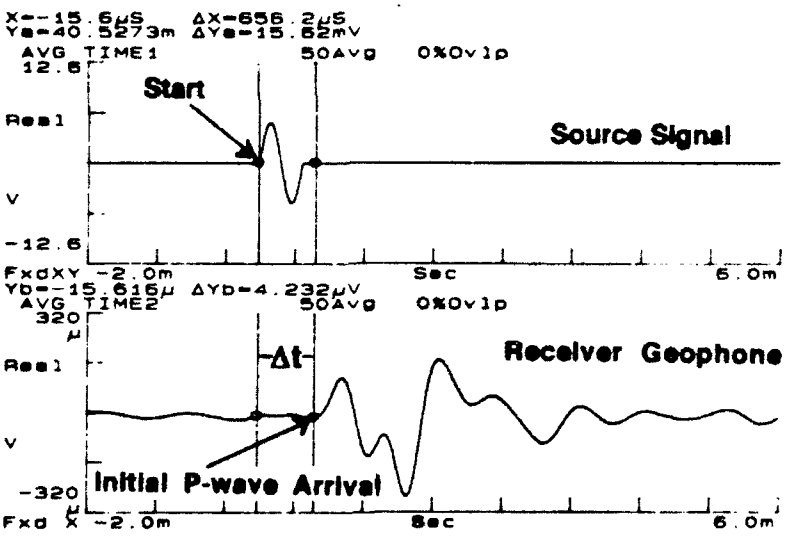

Figure 3.27: Typical Time Response for P-Wave Source and Receiver Geophone 17 from Seismic Testing on 12 August 1992 with an Added Surface Load of 10,200

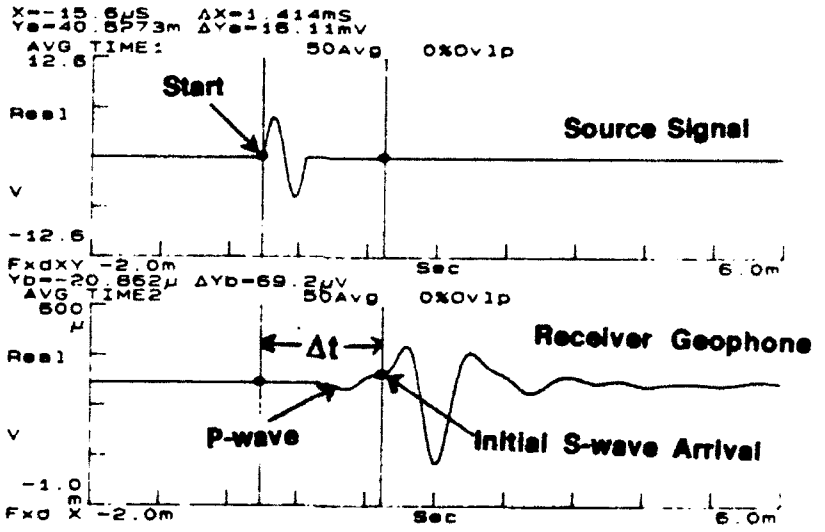

Figure 3.28: Typical Time Response for SH-Wave Source (Geophone 2) and Receiver Geophone (Geophone 17) from Seismic Testing on 12 August 1992 with an Added Surface Load of 10,200

After sufficient data was recorded for the unloaded pavement, the process was then repeated with various static overburden stresses, using known vehicle weights loaded on different rigid plates as listed in Table 3.5. One plate was the wheel load scale, which was 12 in. by 18 in. In other tests, a steel plate 18 in. square was used. In one test a jack was used with an area of 16 sq. in. An 8-ton, single axle dump truck was rented with a driver to apply a static load to the pavement.

This phase of the testing began with the truck empty. The previously described procedures were followed to obtain the time records for each pair of geophones with this added stress. During each subsequent test cycle, more weight was added to the dump truck and the testing continued. Negative pore water pressures were measured only once each testing day. No change was found.

Dates	Weight (lbs)	Area of Plate (in^2)
18 Jul 92	No Load	N/A
10 Aug 92	No Load	N/A
11 Aug 92	4550	216
11 Aug 92	5000	16
12 Aug 92	4700	216
12 Aug 92	8500	216
12 Aug 92	10,200	216
12 Aug 92	11,200	216
12 Aug 92	13,200	324
12 Aug 92	15,000	324

Table 3.5: Dates, Weights and Plates Used in the Seismic Testing When Additional Loads Were Placed on the Pavement Surface

CHAPTER 4
ANALYSIS OF DATA

Installation of the geophones was completed on 20 June 1992. The first lift of asphalt was placed that same day. Construction of all but the top 2-in. (5 cm) lift of asphalt was completed on 10 July 1992. Seismic testing was performed on 18 July, and 10 - 12 Aug 1992. Further, it is planned that the testing will continue every few months over the next two years by other research assistants to determine the effects of time and moisture changes on the stiffness of the soil subgrade.

Using the wave velocities, surface load measurements, and the unit weight of the soil, the resilient moduli under various loads and changes in the state of stress of the soil subgrade were evaluated.

4.1 Determination of the Wave Velocities: Using the time records from the seismic testing, the travel times were determined as described in Section 3.4. The travel times were corrected with the respective calibration factors, as shown in the following equation:

$$\Delta t = t_2 - t_1 - t_c \qquad \text{4.1}$$

where t_1 is the time of arrival of the source wave form, t_2 is the time of arrival of the receiver wave form, and t_c is the calibration factor. As an example, the travel time for the P-wave determined from Figure 3.27 is 0.656 ms ($t_2 - t_1$). The calibration factor for this

geophone pair is 0.076 ms. Therefore, the corrected P-wave travel time is 0.580 ms.

With the corrected travel times and the distances between the respective geophone pairs, the wave velocities were calculated by:

$$V_p = L/\Delta t \quad \text{4.2}$$

and,

$$V_s = L/\Delta t \quad \text{4.3}$$

where V_p is the P-wave velocity, V_s is the S-wave velocity, Δt is the corrected travel time associated with each wave, and L is the near-edge to near-edge spacing of the respective geophones (see Figure 3.9 and Table 3.3). A typical P-wave velocity calculation for geophone pair 1/17 from the time response curve shown in Figure 3.27 (testing performed on 12 Aug. 1992 with 10,200 lb/45.3 KN induced surface load) is as follows:

$$V_p = 0.786\text{ft}/0.580 \times 10^{-3}\text{sec} = 1355\text{ ft/sec } (413.0\text{ m/sec}) \quad \text{4.4}$$

A typical SH-wave velocity calculation for the geophone pair 2/5 from the time response curve shown in Figure 3.28 (testing performed on 12 Aug. 1992 with 10,200 lb/45.3 KN induced surface load) is shown below. The wave velocities for all tests are listed in Tables 4.1 through 4.10.

$$V_s = 0.72\text{ft}/1.322 \times 10^{-3}\text{sec} = 545\text{ ft/sec } (166.1\text{ m/sec}) \quad \text{4.5}$$

4.2 Calculation of Shear and Constrained Moduli of the Soil Subgrade: Using the shear and constrained compression wave velocities and the soil mass density, ρ, the shear modulus, G, and the constrained modulus, M, can be determined for each set of measurements. The wave velocities and respective moduli of the soil under the various loading conditions are listed in Tables 4.1 through 4.10. With the constrained modulus or shear modulus, Poisson's ratio, ν, and the modulus of elasticity, E, can then be estimated as discussed in Section 4.3.

The soil mass density, which is used in the moduli calculations, was calculated to be 3.76 lb-sec^2/ft^4 (1926 kg/m^3). It was found by dividing the total unit weight of the soil (121.2 pcf /19,038 N/m^3 as calculated in Section 3.2.2) by the acceleration due to gravity (32.2 ft/sec^2/9.81 m/sec^2).

The shear modulus, G, is calculated for a typical SH-wave geophone pair, 2/5, for measurements made on 18 July 1992 with no induced load, using Equation 2.5, by:

$$G = (572\text{ft/sec})^2(3.76\text{lb-sec}^2/\text{ft}^4) = 1230\text{ ksf} = 8540\text{ psi (58.9 MPa)} \quad \text{4.6}$$

The constrained modulus, M, is calculated for a typical P-wave geophone pair, 1/17, for measurements made on 18 July 1992 with no induced load, using Equation 2.6, by:

$$M = (1301\text{ft/sec})^2(3.76\text{lb-sec}^2/\text{ft}^4)$$

$$= 6364\text{ ksf} = 44{,}200\text{ psi (304.8 MPa)} \quad \text{4.7}$$

Wave Type	Geophone Pair	Total Travel Time (ms)	Calibration Factor (ms)	Wave Velocity (fps)	Modulus Type	Modulus (ksi)
P	8-9	1.297	0.093	1203.	M	37.80
SH	7-8	2.059	0.172	650	G	11.03
SH	11-12	2.445	0.206	584	G	8.91
SV	13-14	2.297	0.150	602	G	9.46
SH	2-5	1.348	0.092	572	G	8.54
P	1-17	0.679	0.076	1301	M	44.20

Table 4.1: Wave Velocities and Moduli for Different Geophone Pairs (18 Jul. 92 - No Additional Surface Load)

Wave Type	Geophone Pair	Total Travel Time (ms)	Calibration Factor (ms)	Wave Velocity (fps)	Modulus Type	Modulus (ksi)
P	8-9	1.297	0.093	1203	M	37.80
SH	7-8	2.113	0.172	632	G	10.43
SH	11-12	2.504	0.206	569	G	8.45
SV	13-14	2 437	0.150	565	G	8.34
SH	2-5	1.410	0.092	545	G	7.76
P	1-17	0.679	0.076	1301	M	44.20

Table 4.2: Wave Velocities and Moduli for Different Geophone Pairs (10 Aug. 92 - No Additional Surface Load)

Wave Type	Geophone Pair	Total Travel Time (ms)	Calibration Factor (ms)	Wave Velocity (fps)	Modulus Type	Modulus (ksi)
P	8-9	1.305	0.093	1195	M	37.29
SH	7-8	2.102	0.172	635	G	10.53
SH	11-12	2.512	0.206	567	G	8.39
SV	13-14	2.480	0.150	555	G	8.04
SH	2-5	1.410	0.092	545	G	7.76
P	1-17	0.672	0.076	1319	M	45.43

Table 4.3: Wave Velocities and Moduli for Different Geophone Pairs (11 Aug. 92 - Additional Surface Load of 4550 lbs)

Wave Type	Geophone Pair	Total Travel Time (ms)	Calibration Factor (ms)	Wave Velocity (fps)	Modulus Type	Modulus (ksi)
P	8-9	1.340	0.093	1161	M	35.20
SH	7-8	2.094	0.172	638	G	10.63
SH	11-12	2.550	0.206	558	G	8.13
SV	13-14	2.500	0.150	550	G	7.90
SH	2-5	1.418	0.092	542	G	7.67
P	1-17	0.656	0.076	1354	M	47.87

Table 4.4: Wave Velocities and Moduli for Different Geophone Pairs (11 Aug. 92 - Additional Surface Load of 5000 lbs)

Wave Type	Geophone Pair	Total Travel Time (ms)	Calibration Factor (ms)	Wave Velocity (fps)	Modulus Type	Modulus (ksi)
P	8-9	1.297	0.093	1203	M	37.80
SH	11-12	2.523	0.206	564	G	8.31
SV	13-14	2.461	0.150	559	G	8.16
SH	2-5	1.414	0.092	544	G	7.73
P	1-17	0.711	0.076	1238	M	40.02

Table 4.5: Wave Velocities and Moduli for Different Geophone Pairs (12 Aug. 92 - Additional Surface Load of 4700 lbs)

Wave Type	Geophone Pair	Total Travel Time (ms)	Calibration Factor (ms)	Wave Velocity (fps)	Modulus Type	Modulus (ksi)
P	8-9	1.336	0.093	1165	M	35.44
SH	7-8	2.109	0.172	633	G	10.46
SH	11-12	2.516	0.206	566	G	8.36
SV	13-14	2.469	0.150	557	G	8.10
SH	2-5	1.422	0.092	541	G	7.64
P	1-17	0.672	0.076	1319	M	45.43

Table 4.6: Wave Velocities and Moduli for Different Geophone Pairs (12 Aug. 92 - Additional Surface Load of 8500 lbs)

Wave Type	Geophone Pair	Total Travel Time (ms)	Calibration Factor (ms)	Wave Velocity (fps)	Modulus Type	Modulus (ksi)
P	8-9	1.391	0.093	1116	M	32.52
SH	7-8	2.164	0.172	616	G	9.91
SH	11-12	2.539	0.206	560	G	8.19
SV	13-14	2.586	0.150	530	G	7.33
SH	2-5	1.414	0.092	544	G	7.73
P	1-17	0.656	0.076	1354	M	47.87

Table 4.7: Wave Velocities and Moduli for Different Geophone Pairs (12 Aug. 92 - Additional Surface Load of 10,200 lbs)

Wave Type	Geophone Pair	Total Travel Time (ms)	Calibration Factor (ms)	Wave Velocity (fps)	Modulus Type	Modulus (ksi)
P	8-9	1.312	0.093	1188	M	36.85
SH	7-8	2.148	0.172	621	G	10.07
SH	11-12	2.531	0.206	562	G	8.25
SV	13-14	2.484	0.150	554	G	8.01
SH	2-5	1.437	0.092	534	G	7.45
P	1-17	0.672	0.076	1319	M	45.43

Table 4.8: Wave Velocities and Moduli for Different Geophone Pairs (12 Aug. 92 - Additional Surface Load of 11,200 lbs)

Wave Type	Geophone Pair	Total Travel Time (ms)	Calibration Factor (ms)	Wave Velocity (fps)	Modulus Type	Modulus (ksi)
P	8-9	1.297	0.093	1203	M	37.80
SH	7-8	2.133	0.172	625	G	10.20
SH	11-12	2.539	0.206	560	G	8.19
SV	13-14	2.500	0.150	550	G	7.90
SH	2-5	1.422	0.092	541	G	7.64
P	1-17	0.633	0.076	1411	M	51.99

Table 4.9: Wave Velocities and Moduli for Different Geophone Pairs (12 Aug. 92 - Additional Surface Load of 13,200 lbs)

Wave Type	Geophone Pair	Total Travel Time (ms)	Calibration Factor (ms)	Wave Velocity (fps)	Modulus Type	Modulus (ksi)
P	8-9	1.320	0 093	1180	M	36.36
SH	7-8	2.141	0.172	623	G	10.13
SH	11-12	2.523	0.206	564	G	8.31
SV	13-14	2.445	0.150	563	G	8.28
SH	2-5	1.422	0.092	541	G	7.64
P	1-17	0.656	0.076	1354	M	47.87

Table 4.10: Wave Velocities and Moduli for Different Geophone Pairs (12 Aug. 92 - Additional Surface Load of 15,000 lbs)

4.3 Calculation of Poisson's Ratios and Resilient Moduli of the Soil Subgrade with No Additional Surface Load: Using the shear wave and constrained wave velocities in the same orientation, Poisson's ratio, ν, can be determined as given in Equation 2.7. A typical calculation using the wave velocities from the geophone pairs 1/17 for a P-wave and 2/5 for an SH-wave from measurements made on 18 July 1992 is as follows:

$$\nu = [0.5\ (1301\text{fps}/572\text{fps})^2 - 1]/[(1301\text{fps}/572\text{fps})^2 - 1] = 0.38 \quad \text{.....4.8}$$

The modulus of elasticity, E, is a function of Poisson's ratio and the shear wave velocity as given in Equation 2.8. A typical calculation using the Poisson's ratio from wave velocities from geophone pairs 1/17 and 2/5 from measurements made on 18 July 1992 is as follows:

$$E = 2(8540\text{psi})(1+0.38) = 23{,}570\ \text{psi}\ (162.5\ \text{MPa}) \quad \text{.....4.9}$$

As discussed earlier in Section 2.4.5, the resilient modulus, M_R, is assumed to be equal to the modulus of elasticity when there is no permanent deformation; therefore, M_R for this set of tests in the vertical direction is 23,570 psi (162.5 MPa).

Average values for Poisson's ratio and resilient modulus for the soil in all three measurement directions were calculated using the average of seismic measurements performed on 18 July 1992 and 10 August 1992. The combinations of P- and S-wave velocities used in the calculations are as follows: 1. for the vertical direction, geophone

pairs 1/17 and 2/5 were used; 2. for the north-south direction, geophone pair 10/11 and 7/8; and 3. for the east-west direction, geophone pairs 8/9 and 11/12. It must be noted that the Poisson's ratio in the north-south direction was assumed to be the same as in the east-west direction (hence 0.35), since geophone number 10 was inoperative. The resulting Poisson's ratios and resilient moduli are given in Table 4.11. As presented in Table 4.11, the moduli differ, showing anisotropy as discussed in the next section.

Orientation	Geophone Pairs		Poisson's Ratio	Modulus of Elasticity (psi)	Resilient Modulus (psi)
	P-Wave	S-Wave			
East-West	8/9	11/12	0.35	23,436	23,436
North-South	*	7/8	0.35	28,970	28,970
Vertical	1/17	2/5	0.38	22,494	22,494

*** No P-wave measurement because of damaged geophone.**

Table 4.11: Comparison of E, M_R and ν in Three Directions Using Average Wave Velocities from Seismic Measurements with No Added Surface Load

4.4 Anisotropy of of the Compacted Soil Subgrade with No Added Surface Loads: Anisotropy in the soil subgrade can result from two sources: one is the particulate skeleton, which is termed structural or inherent anisotropy, and the second is from an anisotropic state of stress, which is termed stress-induced anisotropy. Unfortunately, the seismic measurements resulted in measuring the combination of these two conditions, and therefore neither type of anisotropy can be determined separately.

A direct way to look at the anisotropic state of the soil is to compare the P-wave velocities in orthogonal directions and the S-wave velocities in orthogonal directions. The averaged values of the P- and S-wave velocities from seismic measurements performed

on 18 July 1992 and 10 August 1992 are presented in Table 4.12.

Wave Type	Geophone	*Direction or Plane	Wave Velocity (fps)
P	8-9	east-west	1203
SH	7-8	north-south	641
SH	11-12	east-west	577
SV	13-14	east-west	584
SH	2-5	vertical	559
P	1-17	vertical	1301

* P-waves are sensitive to conditions in a direction, while S-waves are sensitive to conditions in a plane.

Table 4.12: Average Wave Velocities from Seismic Measurements with No Added Surface Load

The two P-waves (from geophones 1/17 in the vertical direction and 8/9 in the east-west direction) had average wave velocities of 1301 fps (397 m/s) and 1203 fps (367 m/s) in the vertical and east-west directions, respectively. The different P-wave velocities show only slight anisotropy. Unfortunately, the P-wave measurement in the north-south direction was not possible. The SH-waves perpendicular to each other in the horizontal plane (from geophones 7/8 in the north-south direction and 11/12 in the east-west direction) show different wave velocities, which represents a complicated anisotropic state. The S-wave velocities in the vertical plane (from geophones 13/14 in the east-west direction and 2/5 in the vertical plane) are within about 5% of each other. This close comparison is expected because the wave velocities should be equal.

4.5 Calculation of State of Stress Under Added Surface Loads Using Layered Pavement Theory: By adding various known loads on top of the pavement on plates of known area (pressure in psi), the states of stress in the soil subgrade can be changed, and the effect on the soil stiffness can be measured with the seismic velocities. To add a surface load, a dump truck was incrementally loaded with increasing weights and driven on top of a wheel-load scale. The load and area of the loaded pavement are known, so that the induced vertical stresses in the soil subgrade can be calculated using layered pavement theory. To use layered pavement theory, the modulus of elasticity must be known for each layer of pavement material. Therefore, surface wave measurements were performed to evaluate the asphalt as discussed in the following section.

4.5.1 Asphalt Modulus of Elasticity from SASW Tests: The modulus of elasticity of the asphalt is required for calculating the vertical stresses induced in the soil at the depth of the geophones by the surface wheel loads. Using the Spectral-Analysis-of-Surface- Waves (SASW) technique as described in Section 3.2.5, the pavement was tested and the phases of the cross-power spectra were recorded. A typical record is presented in Figure 4.1 A full discussion of the theory behind the procedures is not warranted in this paper and the reader is referred to Stokoe et al 1989 and Aouad et al. 1992.

A computer program developed by Professor Stokoe and his graduate students at the University of Texas at Austin, was used to analyze the phase velocities of the surface waves from the phase angles as shown in Figure 4.1a. A typical calculation for a phase velocity at one wavelength is given in Figure 4.1b.

a.

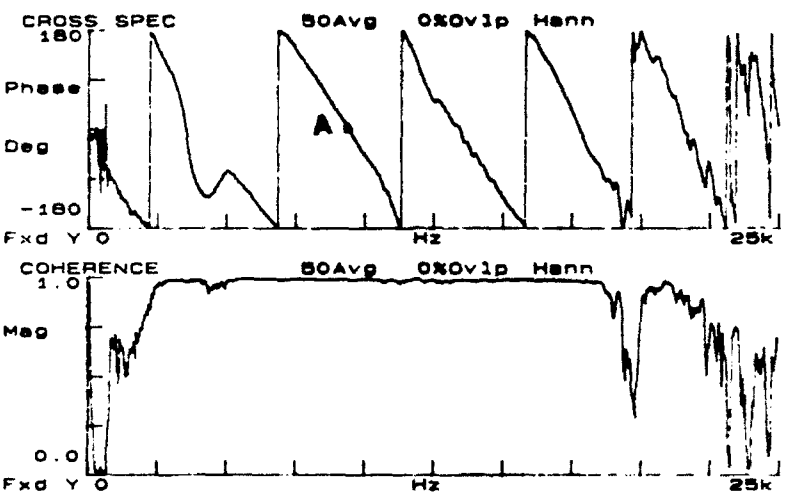

b. Typical Calculation:

At point A:

phase angle, $\phi = 720^{o}$

frequency, f = 9 KHz

receiver spacing, L = 1 ft.

Surface Wave Velocity, $V_R = L\ f\ /(\phi/360)$

V_R = 4500 fps (1372 m/s)

Figure 4.1: (a.) Typical Cross-Power Spectrum and Coherence from SASW Testing and (b.) Typical Calculation of the Surface Wave Velocity at One Wavelength

This calculation is performed for all records, and the plots of velocities versus wavelength (called a dispersion curve) are shown in Figure 4.2. A computer program developed by Professor Roesset and his graduate students at the University of Texas at Austin,was used to model the measured surface wave velocity profile to produce a shear wave velocity profile versus depth. The theoretical match to the measured dispersion is shown in Figure 4.3, and the final shear wave velocity profile is presented in Figure 4.4. The average shear wave velocities for each layer are given in Table 4.13.

Layer Type	Thickness	Vs
Asphalt	2 in.	4300 fps
Asphalt	3 in.	5600 fps
Asphalt	12 in.	5700 fps
Soil Subgrade	4.5 ft.	700 fps

Table 4.13: Average Shear Wave Velocities for Each Layer of Pavement from SASW Testing

By assuming a constant shear wave velocity, V_S, of 5700 fps (1737 m/s) for the entire asphalt thickness and a Poisson's ratio of 0.25, the modulus of elasticity, E, can be calculated for the asphalt using Equation 2.8. It has been shown that the moduli of elasticity found from typical SASW tests on asphalt compared with those found using resonant column and torsional shear tests were four times larger due to the differences in frequency (Aouad et al, 1992). The frequency ranges in those tests were similar to those used in the seismic tests performed in this study; therefore, the modulus of elasticity

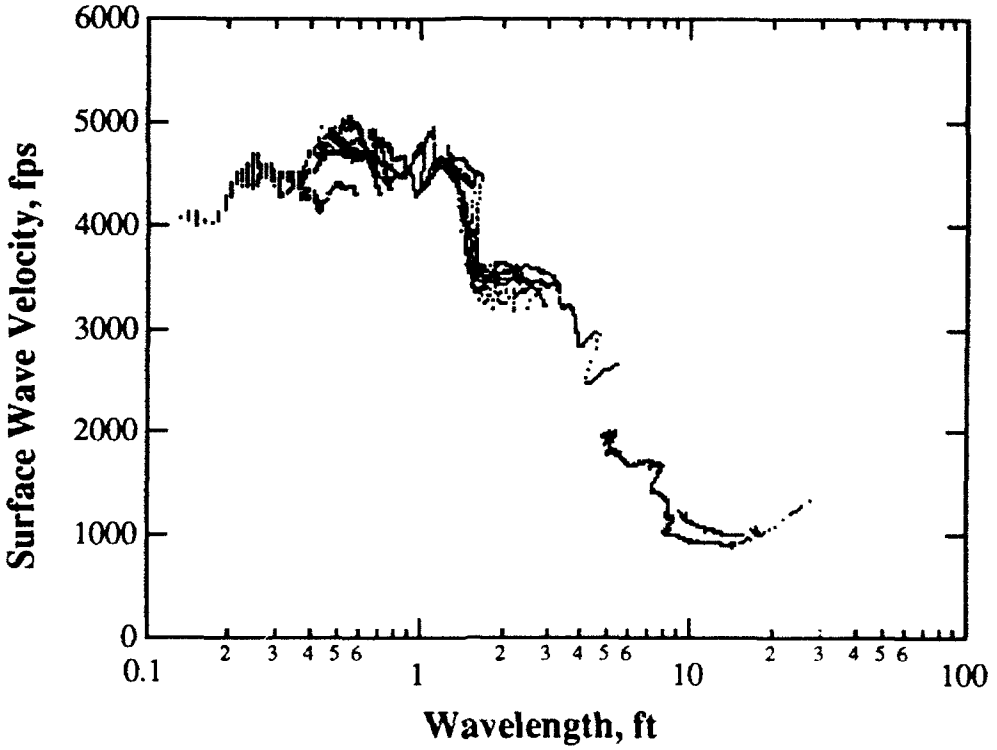

Figure 4.2: Experimental Dispersion Curve for SASW Testing of the Asphalt Pavement

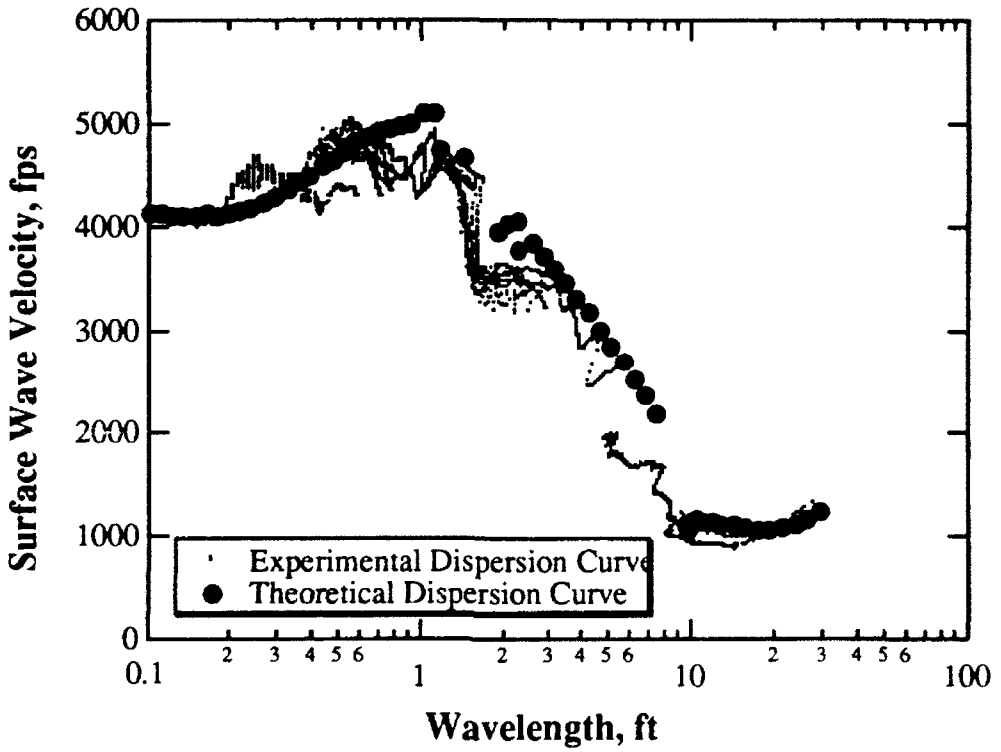

Figure 4.3: Dispersion Curve from SASW Testing with Theoretical Curve Fit

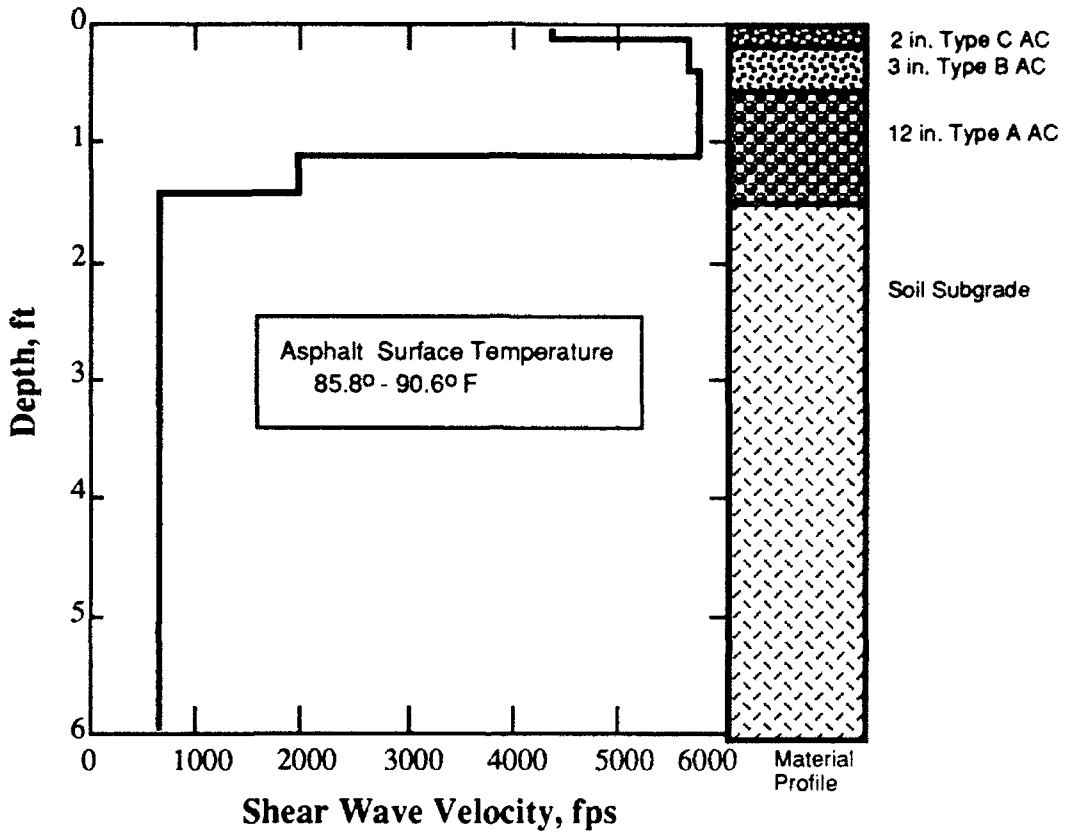

Figure 4.4: Shear Wave Velocity Profile of Asphalt Surface Layer and Underlying Soil Subgrade from SASW Testing

must be reduced by a factor of 4 as follows:

$$E = 2\rho V_s^2 (1 + \nu)/4 \quad \text{.....4.8}$$

$$E = 2(2.6\text{lb-sec}^2/\text{ft}^4)(5700\text{fps})^2 (1 + 0.25)/4$$

$$E = 600{,}000 \text{ psi } (4136.8 \text{ MPa})$$

This modulus is then typical of that value which would be measured with the falling weight deflectometer (FWD).

4.5.2 Vertical Stress Calculations: Using a two-layer model for a pavement system (Yoder and Witczak, 1975), the vertical stresses in the soil at the depths of the geophone array can be calculated. It must be noted that the theory is for the vertical stresses along the centerline directly under the loaded area; however, since the horizontal geophone array is at a depth greater than twice the width of the loaded area, this calculated stress is a good approximation of the increases in vertical effective stress over the entire horizontal geophone array. The two-layer model used in this study is shown in Figure 4.5. A sample analysis using the values shown in Figure 4.5 and the influence chart in Figure 4.6 yields a stress ratio, σ_v/p, of 0.045. In this case, σ_v is the induced vertical stress and p is the stress induced at the surface of the pavement.

The vertical stress induced in the soil equals the stress ratio times the stress induced at the surface of the pavement. A different stress ratio is calculated for each of the different areas of plates as shown in Table 4.14. For geophone pairs 1/17 and 2/5, the average stress was calculated at approximately the mid-depth between the geophones, and the induced vertical stress at the mid-depth of the geophone array was determined by multiplying the stress ratio times the stress induced at the surface of the pavement (see Table 4.15).

As a matter of reference, the largest induced stress increase was about 3 psi (20.7 KPa) at a depth of 31 in. (0.8 m). This corresponds to about 98% of what a standard 18-kip (80 KN) axle load would apply at the same depth.

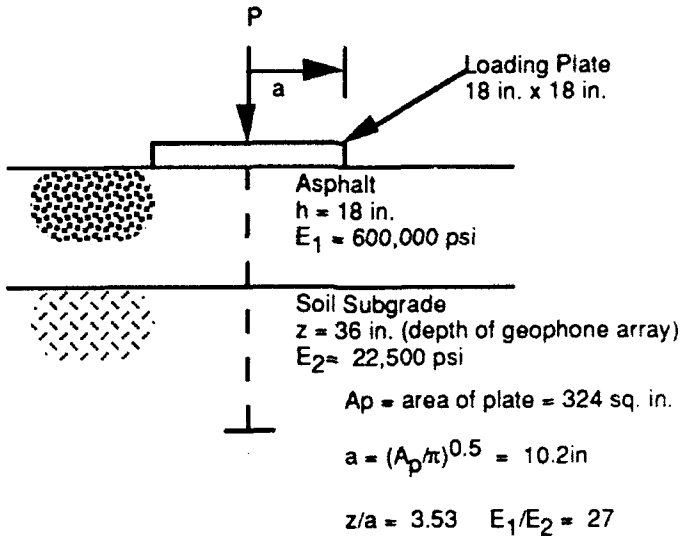

Figure 4.5: Two-Layer Pavement Analysis Model

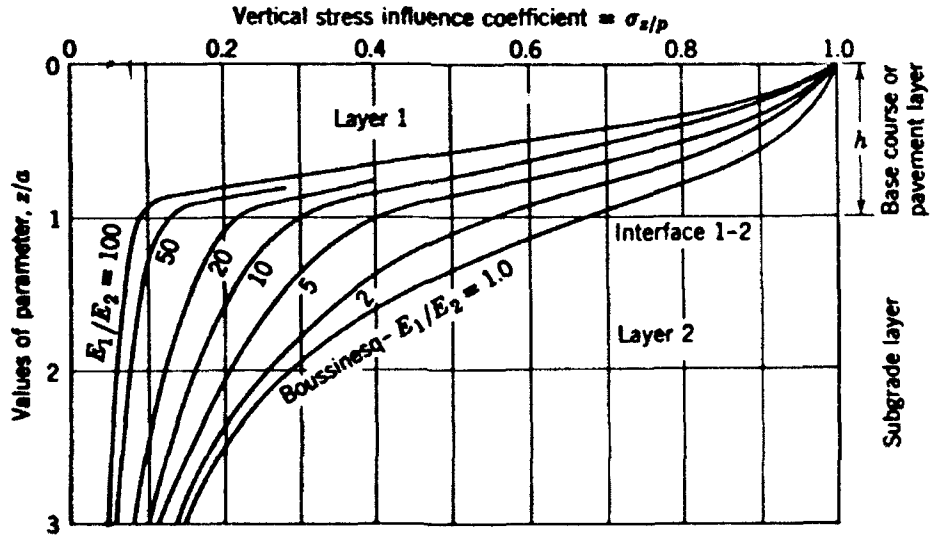

Figure 4.6: Influence Chart for Induced Vertical Stresses in a Two-Layer Pavement Model (Yoder and Witczak, 1975)

Plate Area (in^2)	Stress Ratios (σ_v/p) z = 36 in.	z = 31 in.
324	0.040	0.065
216	0.030	0.040
16	0.005	0.006

Table 4.14: Loading Plate Areas and Stress Ratios

Load (lbs)	Surface Stress (psi)	Induced Vertical Stress (psi) at z = 36 in.	z = 31 in.
4550	21.1	0.63	0.84
5000	312.5	1.56	1.88
4700	21.7	0.65	0.87
8500	39.4	1.20	1.58
10,200	47.2	1.42	1.89
11,200	51.9	1.56	2.08
13,200	40.7	1.63	2.65
15,000	46.3	1.85	3.01

Table 4.15: Induced Loads and Vertical Stresses at the Depth of the Geophone Array

4.5.3 Effective Overburden Stress: The soil at the depth of the geophone array experiences an overburden stress due to the weight of the asphalt and the soil above it. The vertical stress due to the overburden is simply a function of the asphalt unit weight, γ_a, and thickness, h_a, plus the soil unit weight, γ_s, and thickness, h_s, minus the estimated pore water pressure (see Section 3.2.2) from the tensiometer readings, u, (which is negative). Therefore, the effective vertical overburden stress, σ'_v,

before any induced surface loads at the depth of the horizontal geophone array can be calculated by:

$$\sigma_v' = (\gamma_a)(h_a) + (\gamma_s)(h_s) - (-u) \quad \text{4.9}$$

σ_v' = (140pcf)(1.5')/144 + (101.6pcf)(1.5')/144 - (-2.2psi)

σ_v' = 4.7 psi (32.4 KPa)

The effective vertical overburden stress, σ_v', at the mid-depth between geophone pairs 1/17 and 2/5 before any surface loads are added can be calculated by:

σ_v' = (140pcf)(1.5')/144 + (101.6pcf)(1.1')/144 - (-2.2psi)

σ_v' = 4.4 psi (30.3 KPa) 4.10

4.5.4 Induced Horizontal Effective Stresses: The wave velocities in the horizontal plane are affected by changes in the horizontal effective stress. An approximation of the horizontal effective stress was made by using the coefficient of earth pressure at rest:

$$K_o = \nu/(1 - \nu) = 0.35/(1 - 0.35) = 0.54; \quad \text{4.11}$$

where K_o is the ratio of horizontal effective stress to vertical effective stress. A value of 0.5 was used as a reasonable approximation.

Due to the significant compaction effort which occurred in preparing this site by the contractor, it is likely that the initial horizontal effective stresses are on the order of the vertical stresses. If that is assumed, then a sample horizontal stress for an added surface load of 4550 lbs (20.2 KN) can be approximated by:

$$\sigma_h'' = \sigma_h' + 1/2\Delta\sigma_v = \sigma_v' + 1/2\Delta\sigma_v \quad \text{.....4.12}$$

σ_h'' = 4.7psi + 1/2(0.63psi) = 5.0 psi (34.5 KPa)

The vertical effective stresses in the soil at the mid-depth between geophone pairs 1/17 and 2/5 ranged from 4.4 psi (30.3 KPa) to 7.4 psi (51.0 KPa), a difference of 3.0 psi (20.7 KPa), as estimated using the layered pavement model to determine the induced vertical stresses. The resulting horizontal effective stresses are thus estimated to range from 4.4 psi (30.3 KPa) to 5.9 psi (40.7 KPa).

For geophone pair 13/14, with which a horizontally propagating SV-wave was measured, the vertical effective stresses ranged from 4.7 psi (32.4 KPa) to 6.55 psi (45.2 KPa), a difference of 1.85 psi (12.8 KPa). The horizontal effective stresses ranged from 4.7 psi (32.4 KPa) to 5.6 psi (38.6 KPa).

For all the other geophone pairs, the estimated horizontal effective stresses ranged from 4.7 psi (32.4 KPa) to 5.6 psi (38.6 KPa), a difference of 0.93 psi (6.4 KPa).

Because the degree of saturation of the subgrade is estimated to be 79%, it is assumed in the above computations that any induced stress would translate into an equal increase in effective stress.

4.3.4 Effects of Induced Stresses on the Wave Velocities: No measurable changes in wave velocities in the horizontal plane were observed with the estimated changes in the horizontal effective stresses as shown in Figures 4.7, 4.8 and 4.9. This is expected because the horizontal stresses only change from 4.7 psi (32.4 KPa) to 5.6 psi (38.6 KPa), a difference of 0.93 psi (6.4 KPa). Those velocities which only involve horizontal directions are approximately a function of $(\sigma_h)^{0.25}(OCR)^k$ (see Section 4.6 for the explanation of $(OCR)^k$). If the OCR is assumed to be equal to 5 at σ_v = 4.7 psi (32.4 KPa), then the OCR decreases to about 3.6 at σ_v = 6.5 psi (44.8 KPa), corresponding to σ_h = 5.6 psi (38.6 KPa). Hence, the expected change in wave velocity should be on the order of $(5.6psi)^{0.25}(3.6)^{0.14}/(4.7psi)^{0.25}(5))^{0.14}$ = 1.00, or no increase in wave velocity, just as measured.

In the vertical direction, the largest change should be seen in the P-wave velocity with geophone pair 1/17, as shown in Figure 4.10. The expected increase in wave velocity can again be estimated using the ratio of stresses and OCR's, $(7.4psi)^{0.25}(3.2)^{0.14}/(4.4psi)^{0.25}(5))^{0.14}$ = 1.07, or a 7% increase in wave velocity. The measured range of P-wave velocities for geophone pair 1/17 was from approximately 1300 fps (396 m/s) to 1400 fps (427 m/s), an 8% increase with effective vertical stress, which is remarkedly close to the predicted increase.

The shear wave velocities in the vertical plane from geophone pairs 2/5 and 13/14 should have shown some increase in wave velocities with increasing vertical effective stress. Geophone pair 2/5 should have increased by approximately $(7.4psi)^{0.125}(5.9psi)^{0.125}(3.2)^{0.14}/(4.4psi)^{0.25}(5))^{0.14}$ = 1.04, or a 4% increase in wave

velocities. Geophone pair 13/14 should have increased by approximately $(6.5psi)^{0.125}(5.6psi)^{0.125}(3.6)^{0.14}/(4.7psi)^{0.25}(5))^{0.14}$ = 1.02, or a 2% increase in wave velocities. The wave velocities from both geophone pairs remained relatively unchanged with increasing vertical effective stress, as shown in Figures 4.11 and 4.12. The reason(s) for no measurable increases in wave velocities is unknown but is felt to be simply due to scatter in the data.

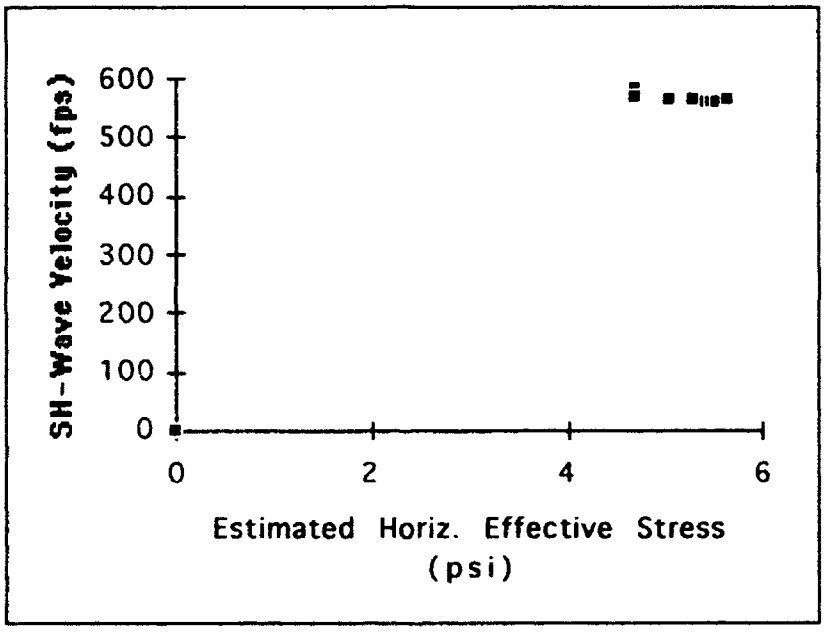

Figure 4.7: P-Wave Velocity Vs. Horizontal Effective Stress for Geophone Pair 8/9; Measurements in the East-West Direction

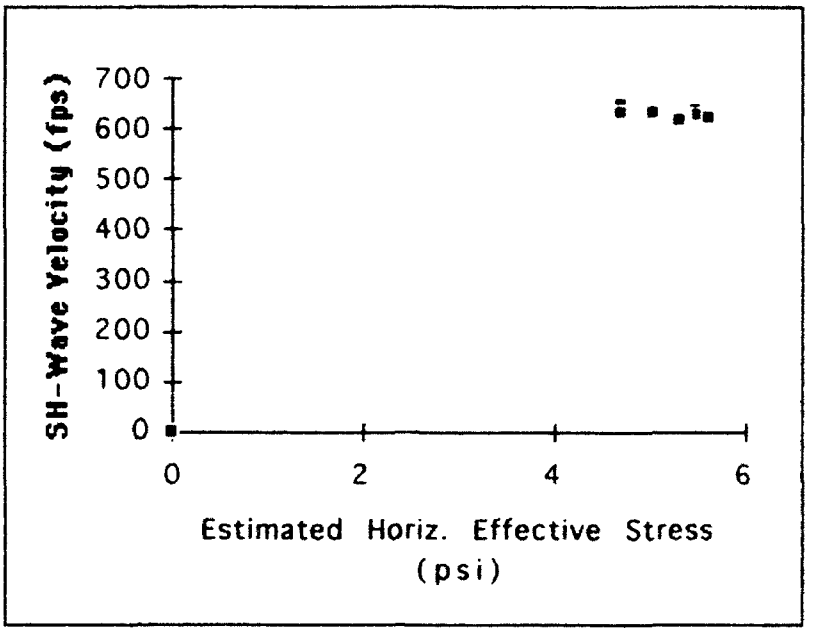

Figure 4.8: SH-Wave Velocity Vs. Horizontal Effective Stress for Geophone Pair 7/8; Measurements in the Horizontal Plane

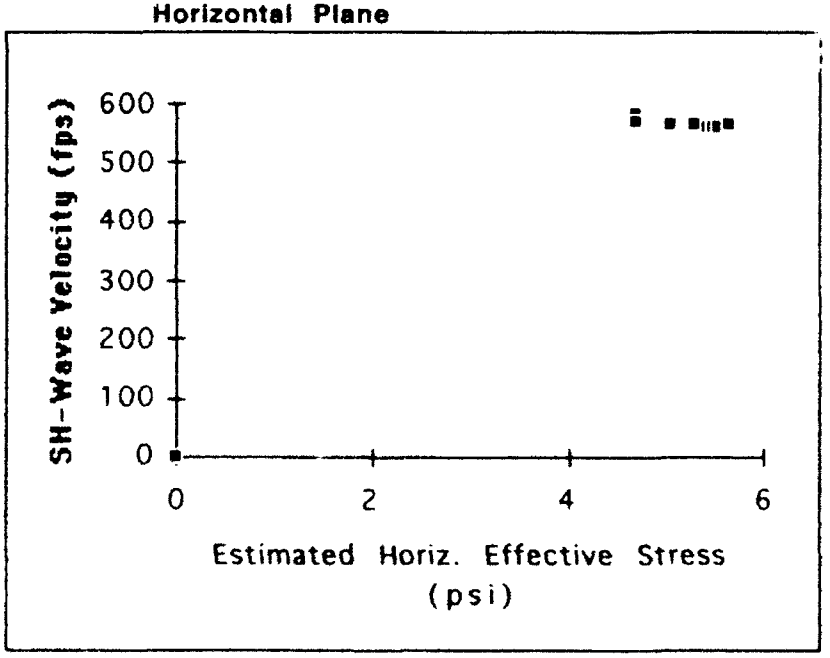

Figure 4.9: SH-Wave Velocity Vs. Horizontal Effective Stress for Geophone Pair 11/12; Measurements in the Horizontal Plane

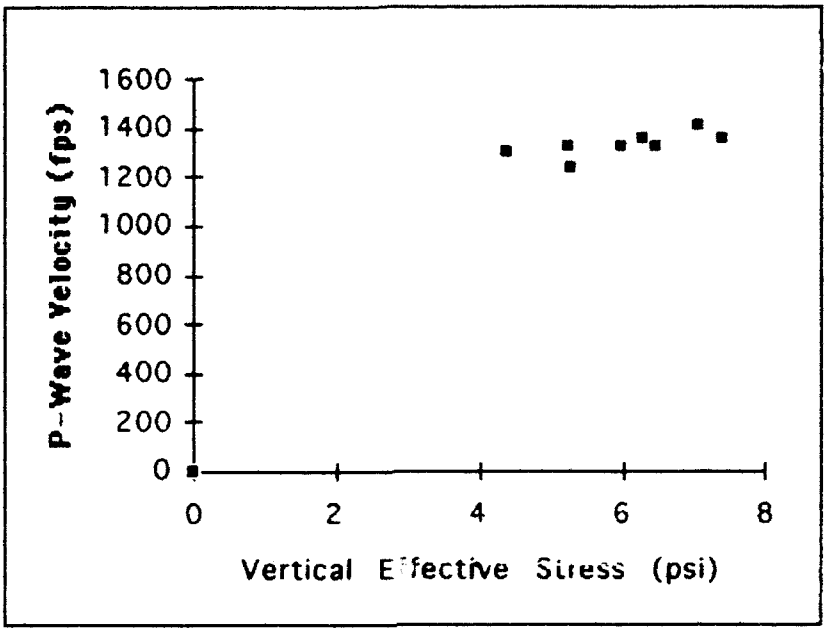

Figure 4.10: P-Wave Velocity Vs. Vertical Effective Stress for Geophone Pair 1/17; Measurements in the Vertical Direction

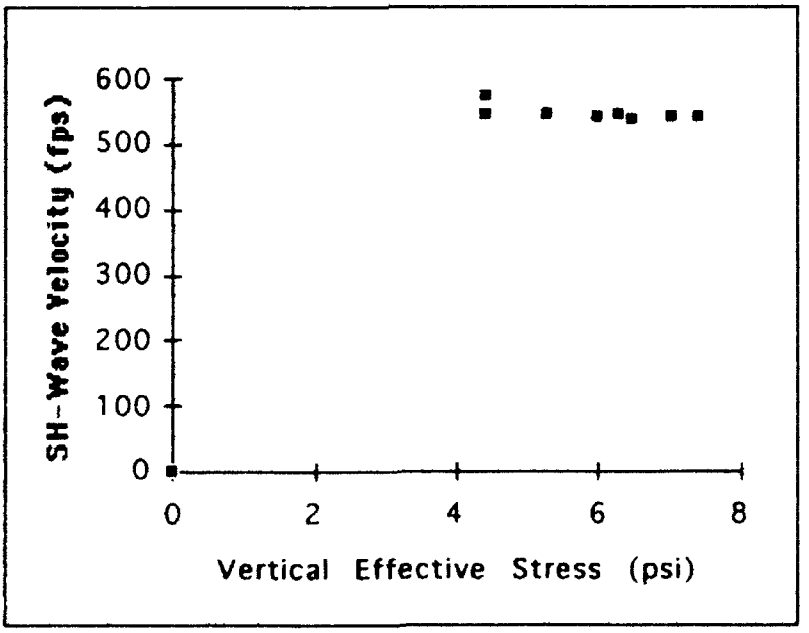

Figure 4.11: SH-Wave Velocity Vs. Vertical Effective Stress for Geophone Pair 2/5; Measurements in the Vertical Plane

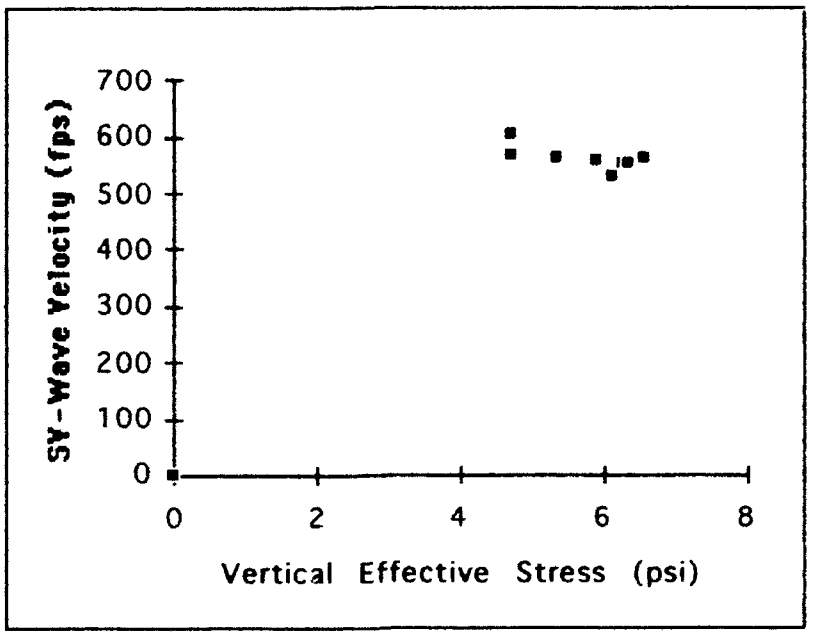

Figure 4.12: SV-Wave Velocity Vs. Vertical Effective Stress for Geophone Pair 13/14; Measurements in the Vertical Plane

Daily weather data, including the high and low temperatures (in degrees Fahrenheit), inches of precipitation and relative humidity (in percent) were recorded from 1 Jul. - 15 Sep. 1992, as shown in Table 4.16. A reporting of "trace" indicated an immeasurable, but detectable amount of precipitation. There were no significant changes in the weather which would have affected the negative pore water pressures in the soil and hence, the wave velocities during the period of testing.

4.6 Comparison of Shear Modulus with the Empirical Maximum Shear Modulus: The calculated shear moduli from this study ranged from 6 - 8 ksi (41.4- 55.2 MPa) as shown in Tables 4.1 - 4.10. The empirical maximum shear modulus, G_{max}, for the soil subgrade is determined using Equation 2.9, where the

Weather Data: 1 July - 15 September 1992

Date	Temp. (F) High	Low	RH %	Prec. (in)
July				
1	95	76	70	0
2	95	80	62	0
3	95	77	68	trace
4	93	69	68	0
5	93	75	60	0
6	94	71	57	0
7	93	74	65	0
8	93	75	57	0
9	93	74	61	0
10	93	77	59	0
11	94	75	55	0
12	93	75	58	0
13	93	75	61	0
14	94	75	57	0
15	96	76	59	0
16	94	77	55	0
17	94	77	63	0
18	95	75	59	0
19	93	71	67	0.32
20	86	71	74	0.37
21	88	72	88	0.11
22	91	74	82	0.09
23	93	75	65	0
24	93	75	61	0
25	93	74	59	0
26	94	74	61	0
27	94	74	57	0
28	94	75	59	0
29	94	75	60	0
30	94	75	61	0
31	95	76	60	0
August				
1	95	74	54	0
2	96	75	52	0.38
3	92	69	52	0.35
4	94	73	59	0
5	95	74	56	0
6	95	74	61	0
7	95	75	61	0
8	95	76	62	0
9	96	77	61	0
10	97	75	60	0
11	99	72	51	0.75
12	92	74	74	0
13	92	76	66	0
14	95	73	52	0
15	88	73	67	trace
16	88	67	49	0
17	89	62	47	0
18	90	66	47	0
19	80	69	58	0.02
20	87	70	64	0
21	93	67	47	0
22	93	68	48	0
23	94	69	57	0.07
24	94	71	60	0
25	96	73	58	0
26	101	744	47	0
27	88	69	90	0.43
28	92	66	44	0
29	94	65	36	0
30	94	65	55	0
31	92	73	61	trace
September				
1	96	74	54	0
2	94	77	57	0
3	98	70	57	0.69
4	95	69	70	0
5	95	75	57	0
6	96	74	65	0
7	95	75	61	0
8	95	75	57	0
9	96	75	57	0
10	96	75	61	0.42
11	91	68	74	0.06
12	91	71	67	0
13	86	72	67	trace
14	91	71	72	0.06
15	91	72	63	0

Table 4.16: Daily Weather Data in Austin TX

overconsolidation ratio (OCR) is estimated at 5, **k** is 0.14 for a PI of 16 (from Table 2.1), the effective vertical stress is 4.7 psi (32.4 KPa) (and is assumed to be equal to the horizontal effective stress) and the void ratio, **e**, is 0.66:

$$G_{max} = \frac{1230\,(2.973 - 0.66)^2(5)^{0.14}(4.7)^{0.5}}{(1+0.66)} = 10{,}770 \text{ psi } (74.3 \text{ MPa}) \cdots\cdots\cdots\cdots 4.10$$

The G_{max} calculated is higher than the typical values of shear modulus calculated from the seismic testing (by about 30%) for reasons unknown but is most likely due to the empirical nature of the equation.

CHAPTER 5

SUMMARY AND CONCLUSIONS

Seismic testing has significant potential for continuous, in-situ determination of the resilient modulus of subgrade and base materials under a highway pavement. The purpose of this study was to develop a method for continuous, in-situ evaluation of the resilient modulus of subgrade material under a highway pavement using seismic waves.

Embedded geophones were successfully employed to measure the shear and constrained moduli and Poisson's ratio in three orthogonal directions. The average wave velocities measured in this study with no added surface load are shown in Table 5.1.

Wave Type	Geophone	*Direction or Plane	Wave Velocity (fps)
P	8-9	east-west	1203
SH	7-8	north-south	641
SH	11-12	east-west	577
SV	13-14	east-west	584
SH	2-5	vertical	559
P	1-17	vertical	1301

* P-waves are sensitive to conditions in a direction, while S-waves are sensitive to conditions in a plane.

Table 5.1: Average Wave Velocities from Seismic Measurements with No Added Surface Load

The resilient modulus, M_R, of the subgrade was equated to the modulus of elasticity since there is no permanent deformation in the soil during seismic testing. In the vertical direction, M_R was found to be approximately 22,500 psi (155 MPa) by measuring the body wave velocities in the subgrade (as shown in Table 5.2).

Orientation	Geophone Pairs P-Wave	Geophone Pairs S-Wave	Poisson's Ratio	Modulus of Elasticity (psi)	Resilient Modulus (psi)
East-West	8/9	11/12	0.35	23,436	23,436
North-South	*	7/8	0.35	28,970	28,970
Vertical	1/17	2/5	0.38	22,494	22,494

*** No P-wave measurement because of damaged geophone.**

Table 5.2: Comparison of E, M_R and ν in Orthogonal Directions Using Average Wave Velocities from Seismic Measurements with No Added Surface Load

The anisotropy of the subgrade under in-situ stress conditions was analyzed by comparing the wave velocities orthogonal planes and directions. The two P-waves (from geophones 1/17 in the vertical direction and 8/9 in the east-west direction) had average wave velocities of 1301 fps (397 m/s) and 1203 fps (367 m/s) in the vertical and east-west directions, respectively. The different P-wave velocities showed only slight anisotropy. Unfortunately, the P-wave measurement in the north-south direction was not possible because of a damaged geophone. The SH-waves perpendicular to each other in the horizontal plane (from geophones 7/8 in the north-south direction and 11/12 in the east-west direction) showed different wave velocities, which represents either a complicated anisotropic state or possible measurement errors. The S-wave velocities in the vertical plane (from geophones 13/14 in the east-west direction and 2/5 in the vertical plane) were within about 5% of each other. This close comparison is expected because the wave velocities should be equal.

The changes in wave velocity with changes in effective stress were analyzed. No measurable changes in wave velocities in the horizontal plane were observed with the estimated changes in the horizontal effective stresses as shown in Figures 4.7, 4.8 and 4.9. This is expected because the horizontal stresses only change from 4.7 psi (32.4 KPa) to 5.6 psi (38.6 KPa), a difference of 0.93 psi (6.4 KPa). Those velocities which only involve horizontal directions are approximately a function of $(\sigma_h)^{0.25}(OCR)^k$. If the OCR is assumed to be equal to 5 at σ_v = 4.7 psi (32.4 KPa), then the OCR decreases to about 3.6 at σ_v = 6.5 psi (44.8 KPa), corresponding to σ_h = 5.6 psi (38.6 KPa). Hence, the expected change in wave velocity should be on the order of $(5.6psi)^{0.25}(3.6)^{0.14}/(4.7psi)^{0.25}(5))^{0.14}$ = 1.00, or no increase in wave velocity, just as measured.

In the vertical direction, the largest change should be seen in the P-wave velocity with geophone pair 1/17, as shown in Figure 4.10. The expected increase in wave velocity can again be estimated using the ratio of stresses and OCR's, $(7.4psi)^{0.25}(3.2)^{0.14}/(4.4psi)^{0.25}(5))^{0.14}$ = 1.07, or a 7% increase in wave velocity. The measured range of P-wave velocities for geophone pair 1/17 was from approximately 1300 fps (396 m/s) to 1400 fps (427 m/s), an 8% increase with effective vertical stress, which is remarkedly close to the predicted increase.

The shear wave velocities in the vertical plane from geophone pairs 2/5 and 13/14 should have shown some increase in wave velocities with increasing vertical effective stress. Geophone pair 2/5 should have increased by approximately $(7.4psi)^{0.125}(5.9psi)^{0.125}(3.2)^{0.14}/(4.4psi)^{0.25}(5))^{0.14}$ = 1.04, or a 4% increase in wave

velocities. Geophone pair 13/14 should have increased by approximately $(6.5psi)^{0.125}(5.6psi)^{0.125}(3.6)^{0.14}/(4.7psi)^{0.25}(5))^{0.14}$ = 1.02, or a 2% increase in wave velocities. The wave velocities from both geophone pairs remained relatively unchanged with increasing vertical effective stress, as shown in Figures 4.11 and 4.12. The reason(s) for no measurable increases in wave velocities is unknown but is felt to be simply due to scatter in the data.

With already proven field techniques and relatively inexpensive equipment, many seismic tests can be run in a short period of time, over the long term, or continuously to determine the resilient modulus of pavement subgrades. As the need for more cost effective pavement designs increases, the degree of accuracy of knowing the properties of the materials increases. In-situ seismic testing will improve the knowledge of some of the most important soil properties used in designing pavement systems.

Appendix A: Sample Time Records Measured During Seismic Testing

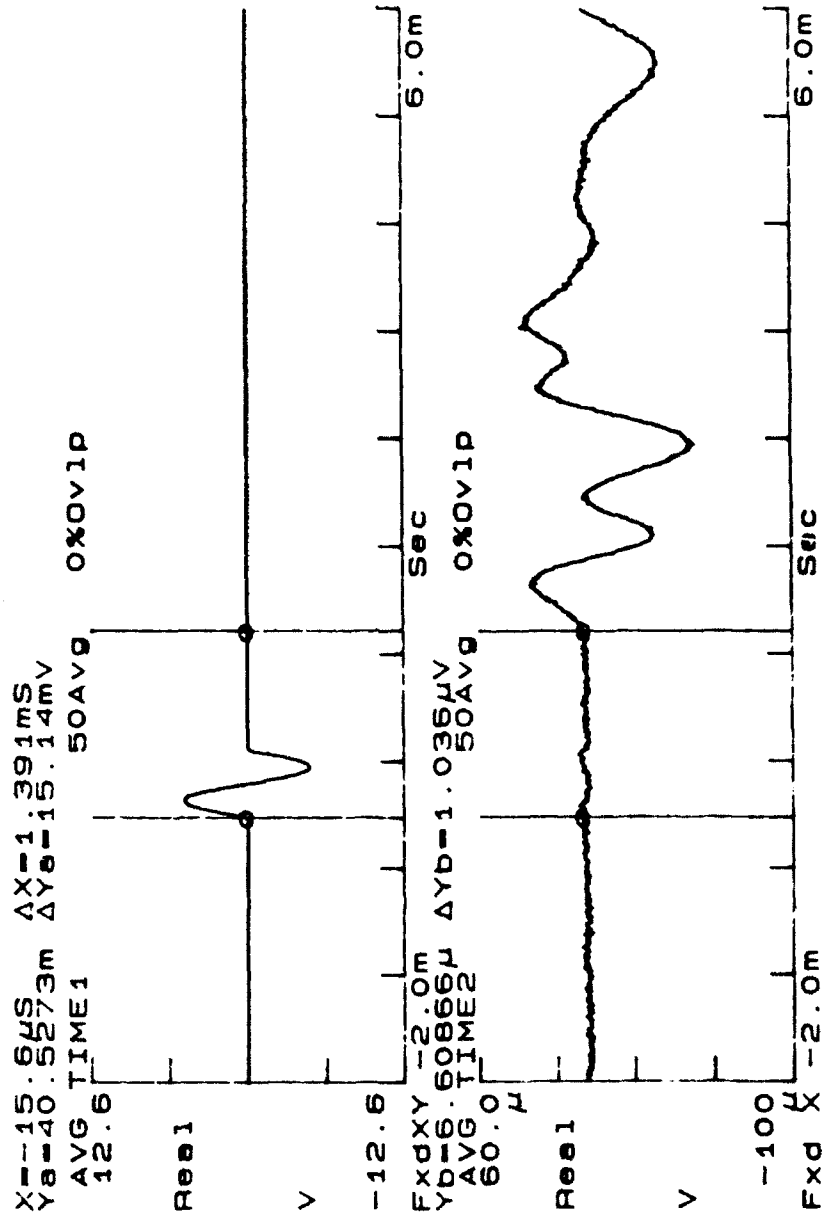

Figure A.1 - Response Curves for 12 Aug 1992 - 10,200 lbs Surface Load; P-Wave: Geophones 8/9

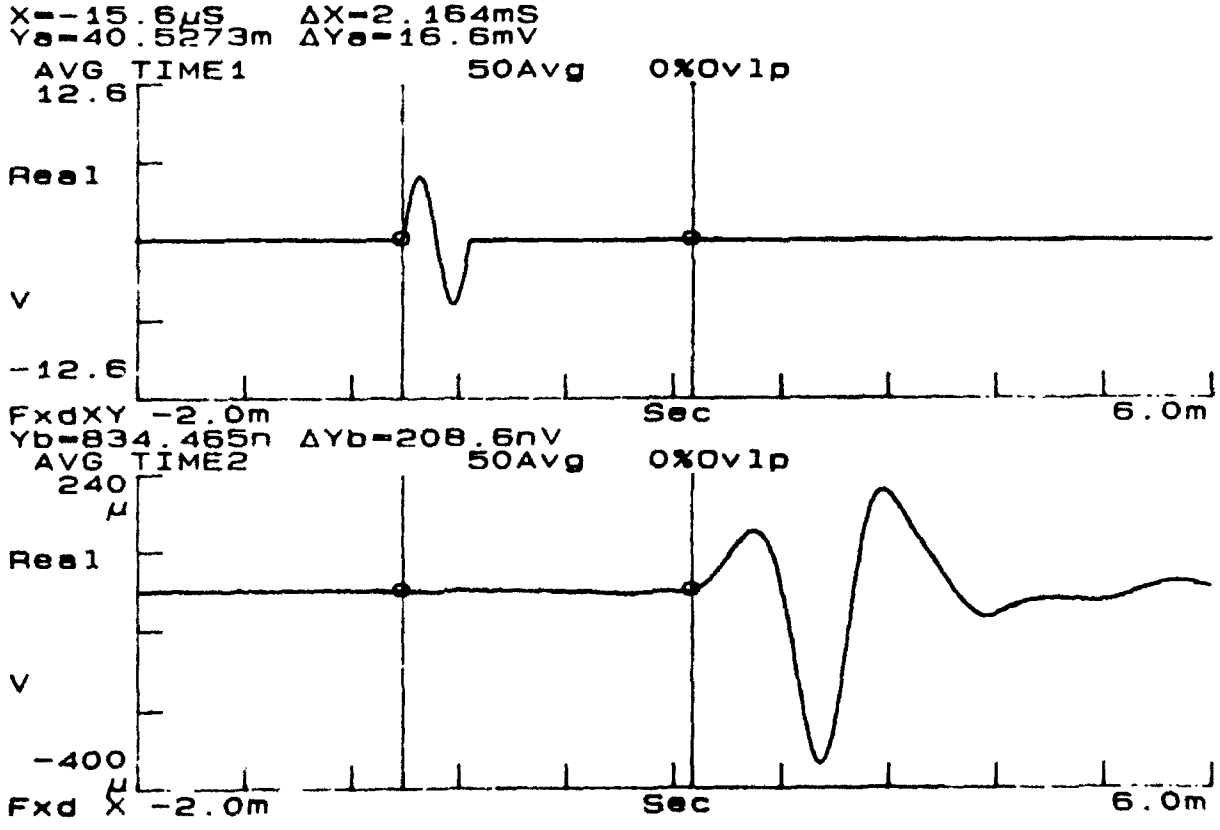

Figure A.2 - Response Curves for 12 Aug 1992 - 10,200 lbs Surface Load; SH-Wave: Geophones 7/8

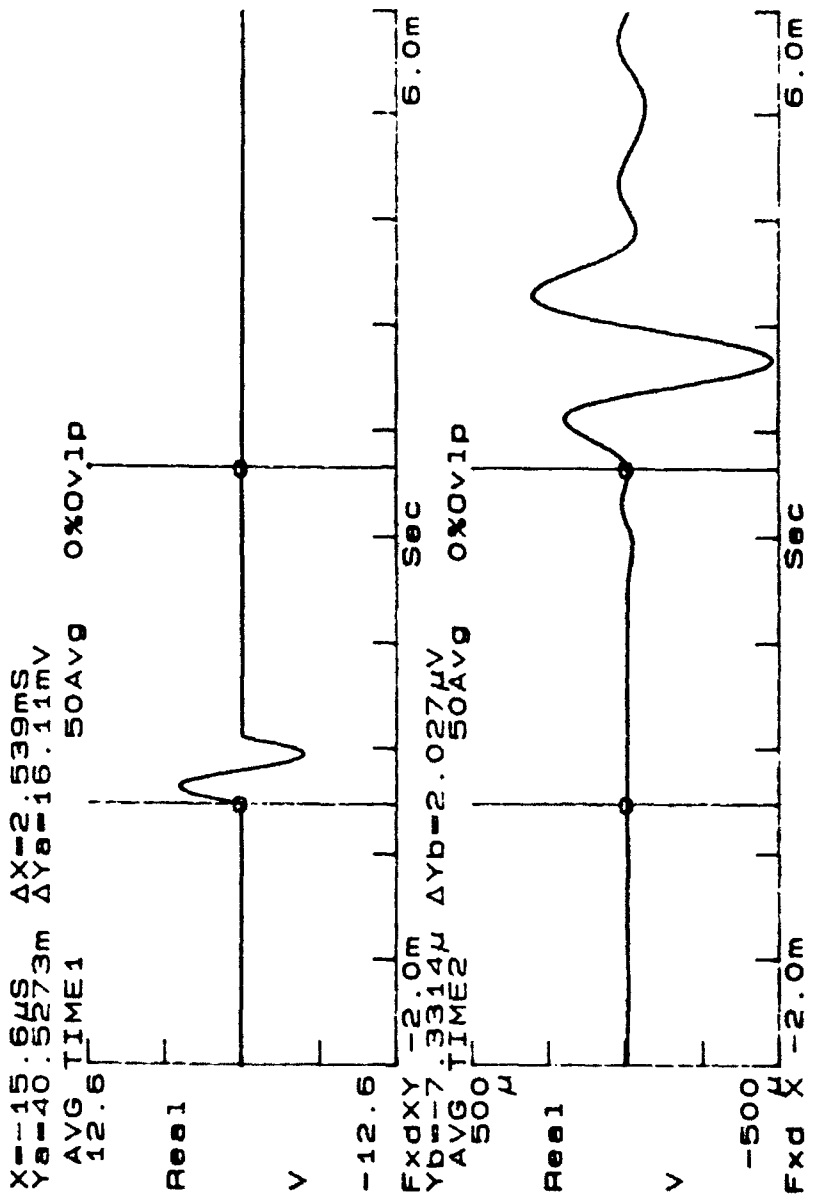

Figure A.3 - Response Curves for 12 Aug 1992 - 10,200 lbs Surface Load; SH-Wave: Geophones 11/12

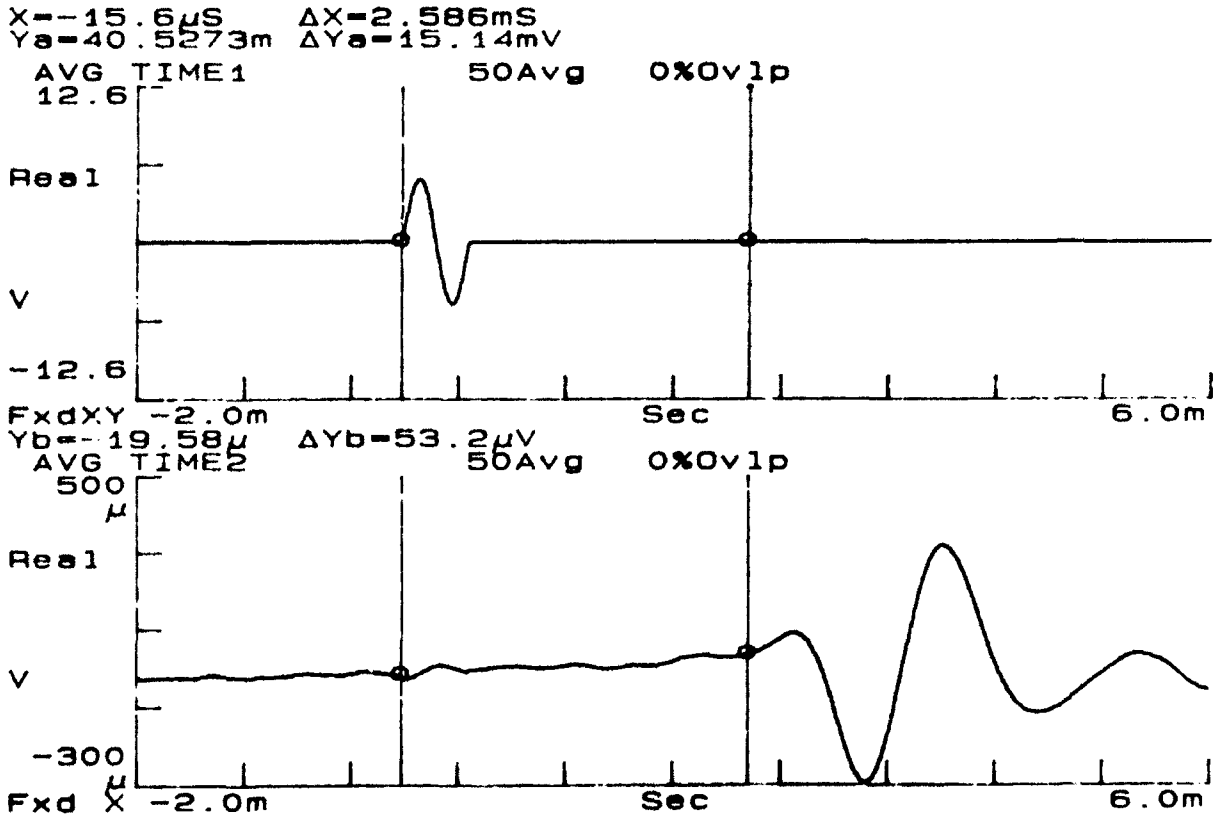

Figure A.4 - Response Curves for 12 Aug 1992 - 10,200 lbs Surface Load; SH-Wave: Geophones 13/14

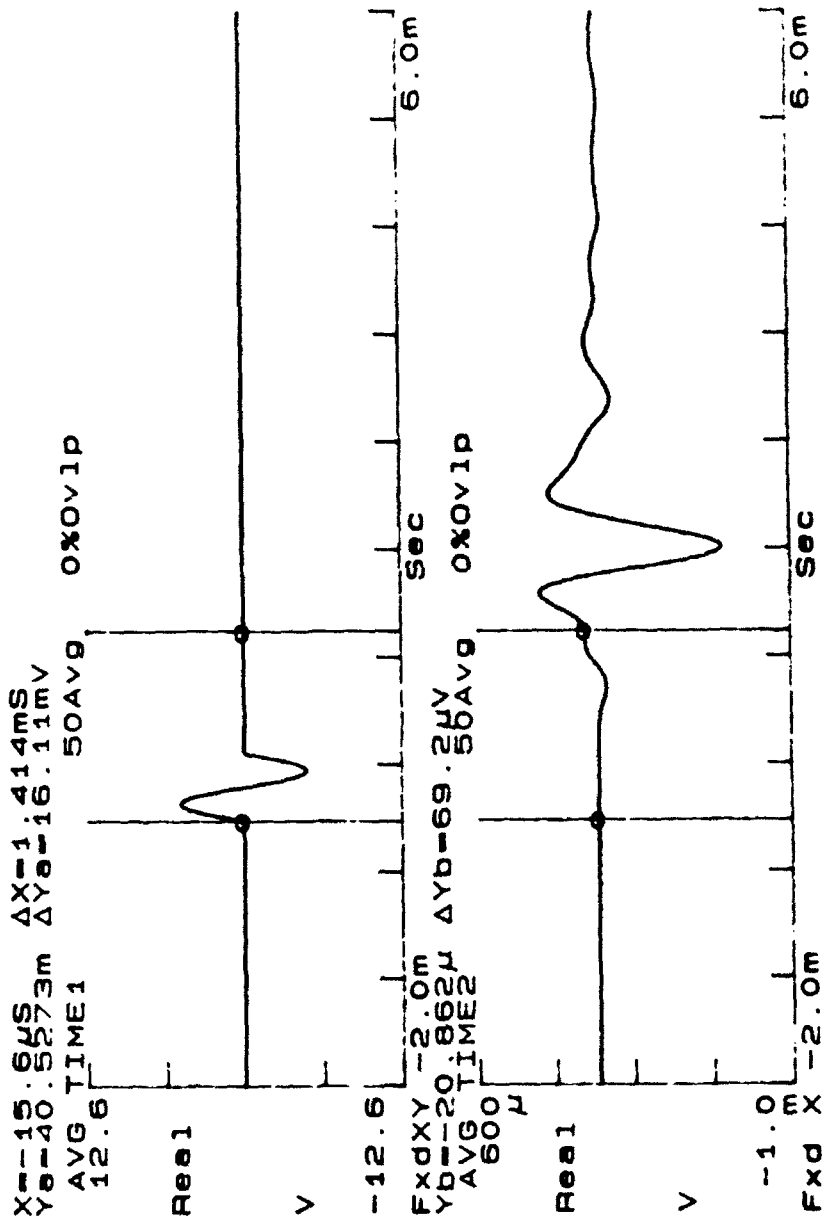

Figure A.5 - Response Curves for 12 Aug 1992 - 10,200 lbs Surface Load; SV-Wave: Geophones 2/5

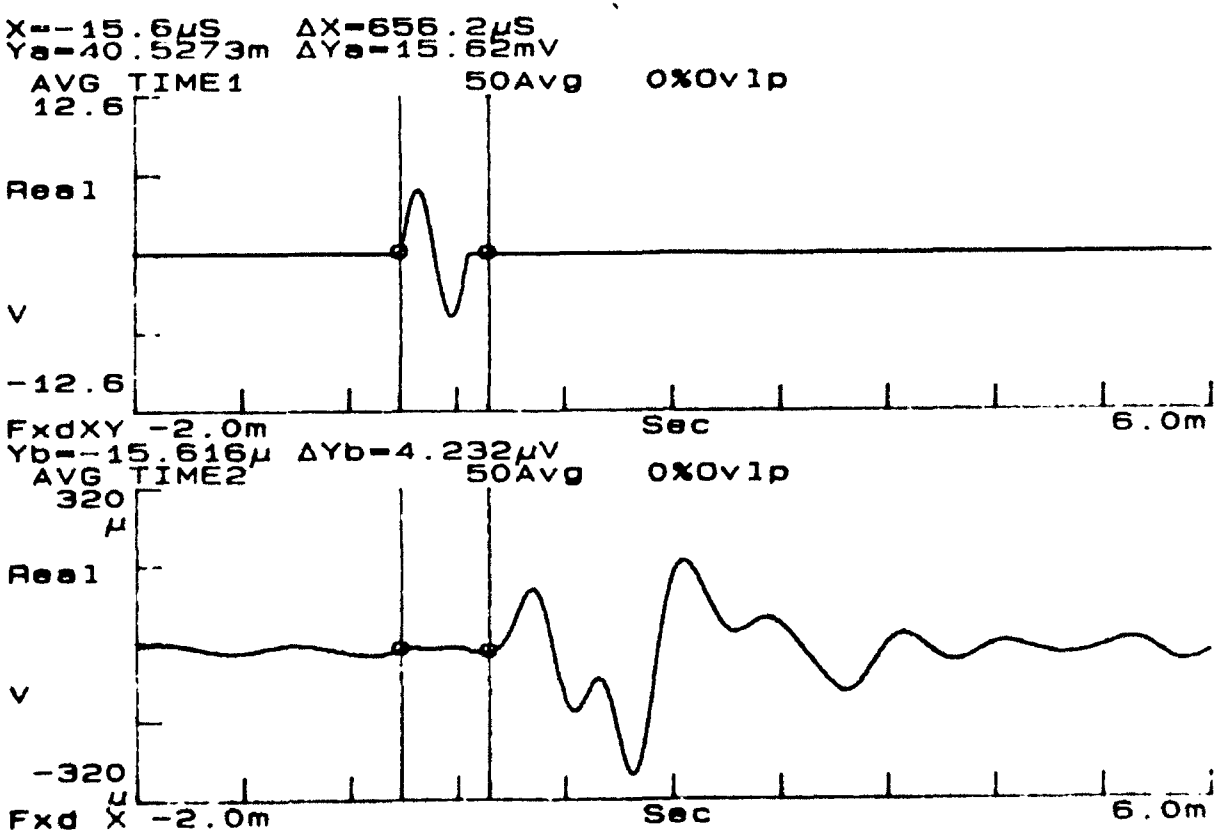

Figure A.6 - Response Curves for 12 Aug 1992 - 10,200 lbs Surface Load; P-Wave: Geophones 1/17

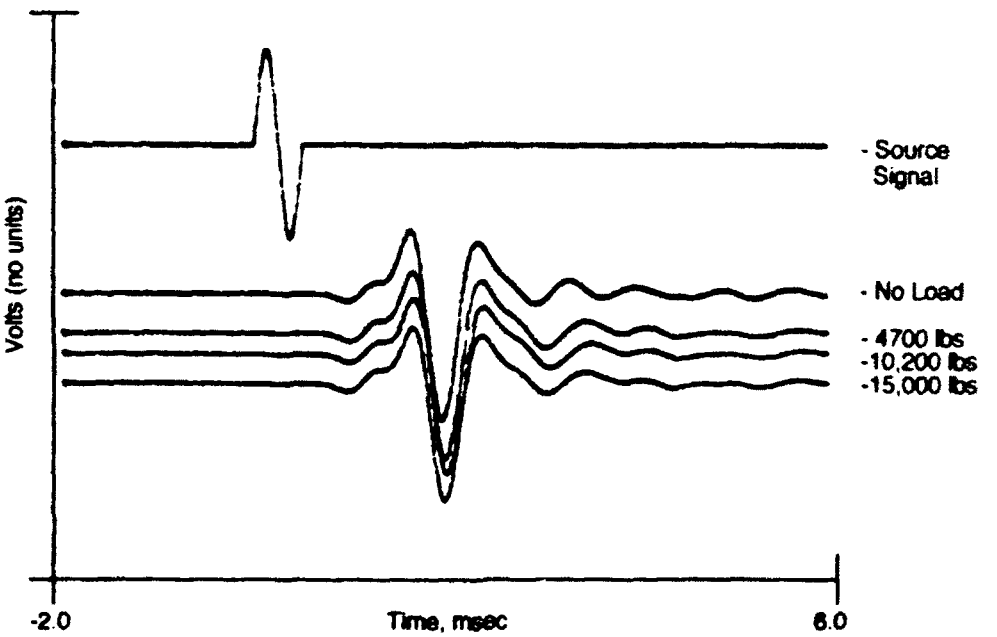

Figure A.7 P-Wave Response Curves for Several Added Surface Loads for Geophone Pair 1/17

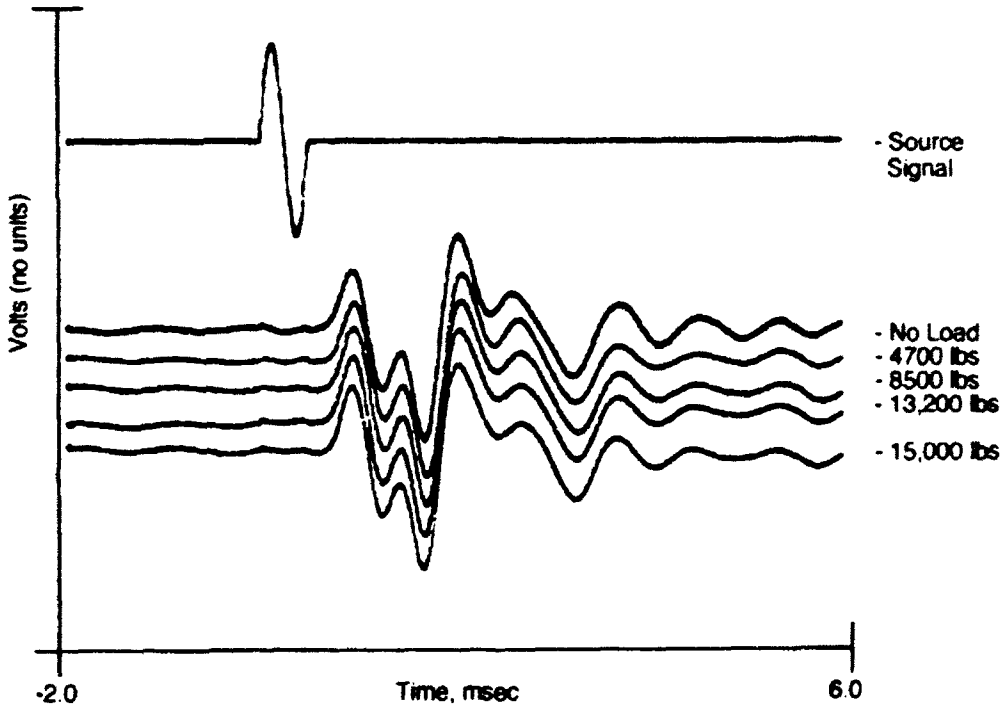

Figure A.8 SH-Wave Response Curves for Several Added Surface Loads for Geophone Pair 2/5

Appendix B: Calibration Curves for Time Delays Associated with Each Geophone Pair

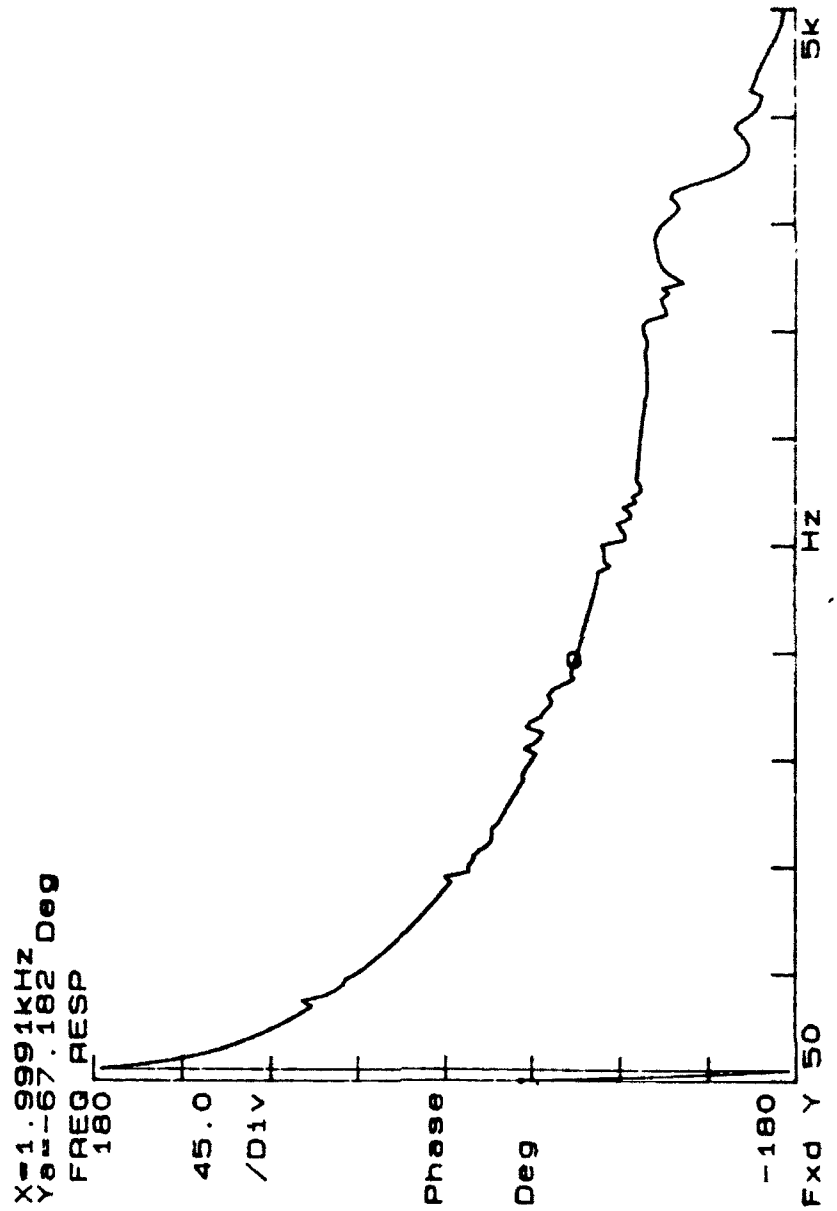

Figure B.1 - Calibration Curve for Time Correction; P-Wave Geophone Pair 8/9

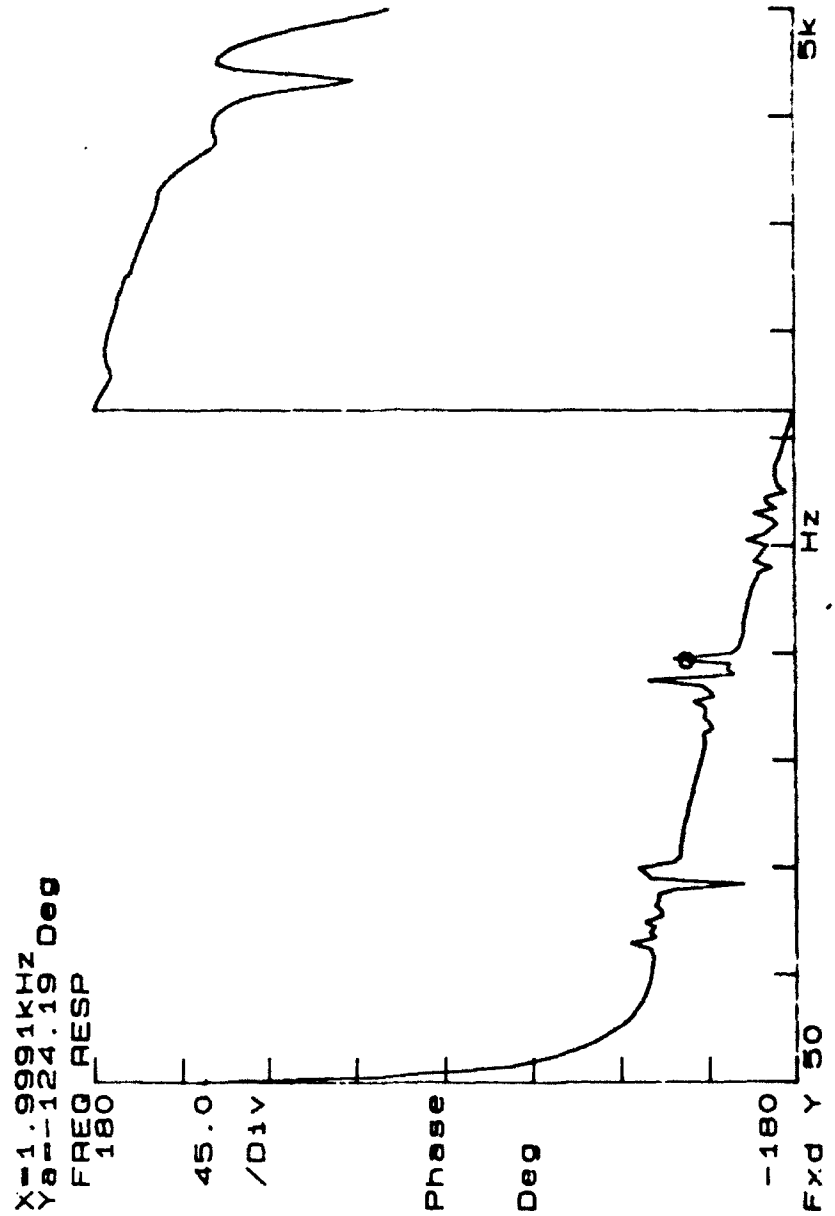

Figure 8.2 - Calibration Curve for Time Correction; SH-Wave Geophone Pair 7/8

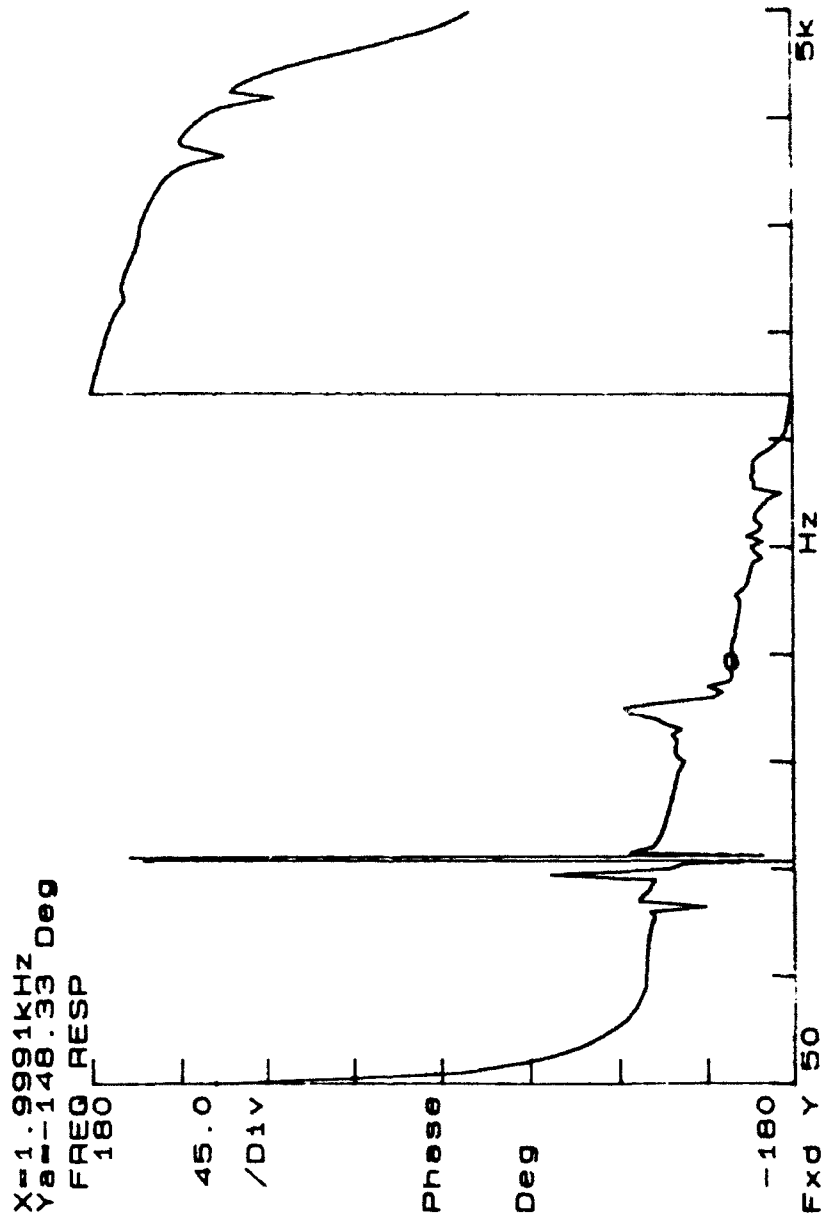

Figure B.3 - Calibration Curve for Time Correction; SH-Wave Geophone Pair 11/12

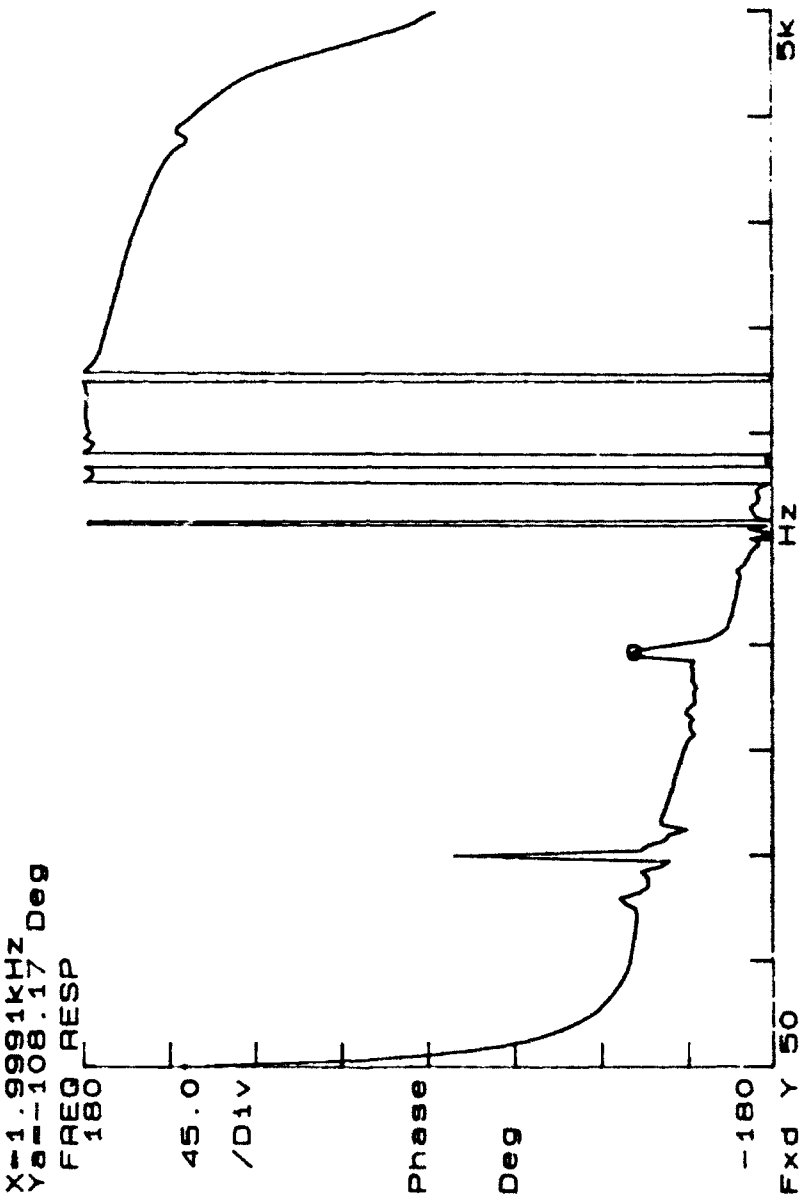

Figure B.4 - Calibration Curve for Time Correction; SV-Wave Geophone Pair 13/14

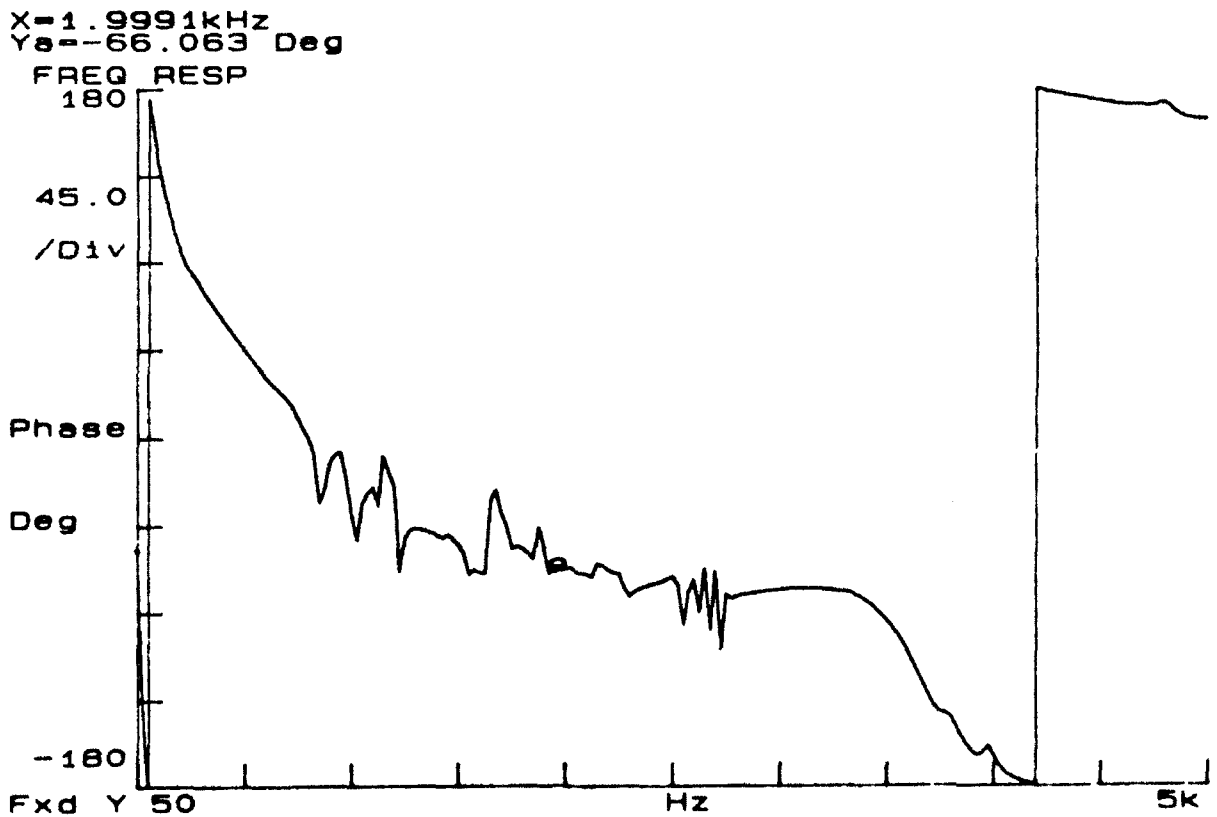

Figure B.5 - Calibration Curve for Time Correction; SH-Wave Geophone Pair 2/5

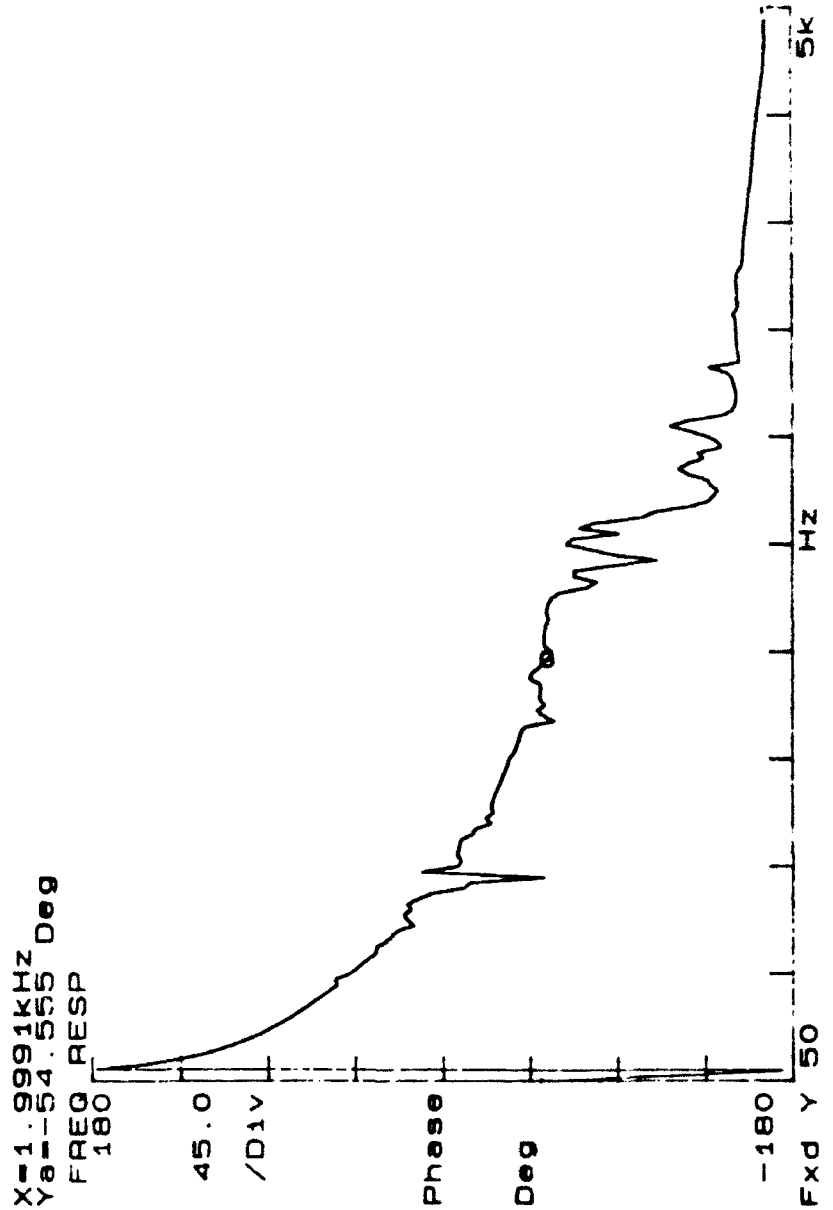

Figure B.8 - Calibration Curve for Time Correction; P-Wave Geophone Pair 1/17

REFERENCES

Aouad, M. F., K. H. Stokoe, II, and R. C. Briggs (1992) *Stiffness of the Asphalt Concrete Surface Layer from Stress Wave Measurements*, Paper Prepared for Presentation to the 1993 Annual Meeting of the Transportation Research Board, University of Texas at Austin

Hardin, B. O. and V. P. Drnevich (1972) *Shear Modulus and Damping in Soils: Design Equations and Curves*, Journal of the Soil Mechanics and Foundations Division, ASCE, Vol. 98, No. SM7, pp. 667-692.

Richart, F. E., Jr., J. R. Hall, Jr., and R. D. Woods (1970) *Vibrations of Soils and Foundations*, Prentice-Hall, Inc., Englewood Cliffs, N. J.

Seed, H. B. and I. M. Idriss (1970) *Soil Moduli and Damping Factors for Dynamic Response Analysis*, Earthquake Engineering Research Center Report, EERC 70-10.

Stannard, David I (1986) *Theory, Construction and Operation of Simple Tensiometers*, Ground Water Monitoring Review, Vol. 6, No. 3, pp. 70-78.

Stokoe, K. H. II, J. N. Lee, and S. H. Lee (1991) *Characterization of Soil in Calibration Chambers with Seismic Waves*, Calibration Chamber Testing, Edited by An-Bin Huang, Proceedings of the First International Symposium on Calibration Chamber Testing/ISOCCTI, Potsdam, N. Y., pp. 363-376.

Stokoe, K. H., II (1980) *Field Measurement of Dynamic Soil Properties*, Presented to the Specialty Conference on Civil Engineering and Nuclear Power, ASCE, Sept. 15-17, Knoxville, TN, 31 p.

Stokoe, K. H., II and R. J. Hoar (1978) *Variables Affecting In Situ Seismic Measurements*, Proceedings of the Conference on In-Situ Measurement of Soil Properties, ASCE, Vol. II, pp. 919-939.

Yoder, E. J. and M. W. Witczak (1975) *Principles of Pavement Design*, 2nd Ed., John Wiley and Sons, Inc., pp. 40-41.

VITA

Captain Michael Paul Rits was born in Grove City, Pennsylvania, on July 17, 1963, the son of Lorraine Weller Rits and Edgar Heckman Rits. After graduating from Juniata High School, Mifflintown, Pennsylvania, in 1981, Michael entered the United States Air Force Academy in Colorado Springs, Colorado. He received the degree of Bachelor of Science in Civil Engineering in May, 1985 and was commissioned as a Second Lieutenant in the United States Air Force. While in the Air Force, he served as a civil engineering officer at Andrews Air Force Base, Maryland, Spangdahlem Air Base, Germany, and in August, 1991, entered The Graduate School of The University of Texas. He will go on to teach civil engineering at the United States Air Force Academy.

Permanent address: R.D. 1
Honey Grove, Pennsylvania 17035